

**Quantification of Performance of Wildfire Chemicals using Custom-Built
Heat Flux Sensors**

by

Shammawi Akeno Altiman Anderson

A thesis submitted in partial fulfillment of the requirements for the degree of

Master of Science

Department of Mechanical Engineering

University of Alberta

© Shammawi Akeno Altiman Anderson, 2016

ABSTRACT

A robust heat flux sensor was developed in order to quantify the energy release from high heat load scenarios, such as wildland fires. In order to reduce the high errors in the heat flux data, the sensor was modified to measure the differential temperature so as to mitigate the propagation of error. Controlled laboratory and field validation tests were performed to verify the reduction in error and the results were compared to those obtained from an unmodified sensor and a commercial heat flux sensor. The capabilities of the improved sensor design were further expanded by application of the sensor to the evaluation of wildfire chemicals. As a result, a simple and effective test methodology was developed for differentiating wildfire chemicals based on the ignition time of foliar vegetative fuel samples. The modified heat flux sensor was used to determine the time to flaming ignition along with the incident heat flux and the results obtained were compared to those obtained from the transient mass loss data measured by a strain gauge-based load cell. Statistical *t*-test analysis was conducted on the time-to-ignition data to determine whether the results were statistically significant for the different chemical treatments. The results indicated that the test methodology allowed for effective differentiation between the wildfire chemical treatments by comparing their mean ignition times. The narrow standard deviations of the mean ignition times suggested that the test methodology was able to produce repeatable results. Based on the custom heat flux sensor design and the developed methodology, a thermal calorimeter was then designed to measure the heat release rate of the foliar vegetative fuel samples, which is considered to be a useful thermal property.

ACKNOWLEDGMENTS

I would like to extend my sincere gratitude to everyone who has supported me along this unforgettable journey. I would like to start by thanking my supervisor, Dr. André McDonald for accepting me into his prestigious research group. He has contributed to a rewarding graduate program experience by giving me continuous support, engaging me in new ideas, and demanding high quality of work in all my endeavors. You have been a tremendous mentor and for that I will be forever indebted.

I would also like to thank the entire FP Innovations team, especially Mr. Ray Ault and Mr. Greg Baxter, for their assistance with the tedious task of collecting experimental data whether it is in the lab or NWT. I would also like to thank Mr. Stephen Paskaluk, Mr. Mark Ackerman, Razim Rafai, and Oleg Melnik, for providing tremendous support along the way. I would also like to thank the administrative staff of the Mechanical Engineering Department for giving me all the necessary assistance during my studies. I would like to thank the entire research group for making my time here an unforgettable experience.

Last, but not least, I would like to thank my family and friends for their unwavering love and support. I am deeply indebted especially to Kimberly and our newborn son, Micah, for providing me with the much needed inspiration. I would also like to specially thank my parents, for their faith in me and allowing me to be as ambitious as I wanted.

“It always seems impossible until it’s done.”

Nelson Mandela

TABLE OF CONTENTS

ABSTRACT	ii
ACKNOWLEDGMENTS	iii
LIST OF FIGURES	vi
LIST OF TABLES	viii
NOMENCLATURE	ix
1. INTRODUCTION	1
1.1 WILDLAND FIRES	1
1.2 WILDLAND FIRE FUEL CHARACTERISTICS	2
1.3 MEASURING ENERGY TRANSFER IN WILDLAND FIRES	4
1.4 WILDFIRE SUPPRESSION CHEMICALS	6
1.5 FIRE CALORIMETRY	8
1.6 OBJECTIVES	13
1.7 THESIS ORGANIZATION.....	14
2. MATHEMATICAL MODELS AND EXPERIMENTAL METHODS	15
2.1 HEAT FLUX SENSOR DEVELOPMENT.....	15
2.2 MODIFIED HEAT FLUX SENSOR DESIGN AND FABRICATION	17
2.3 MODIFIED HEAT FLUX SENSOR VALIDATION.....	20
2.3.1 Electric Powered Radiant Heater Test	20
2.3.2 Mass Loss Calorimeter Test.....	23
2.3.3 Controlled Crown Fire Test	24
2.4 EVALUATION OF WILDFIRE CHEMICALS	26
2.4.1 Wildfire Chemicals Evaluation Apparatus	26
2.4.2 Wildfire Chemicals Evaluation Methodology	27
3. RESULTS AND DISCUSSIONS	30
3.1 ELECTRIC POWERED RADIANT HEATER TEST.....	30
3.2 MASS LOSS CALORIMETER TESTS.....	35
3.3 CONTROLLED CROWN FIRE TEST	40
3.4 UNCERTAINTY ERROR ANALYSIS	42
3.5 WILDLAND FIRE CHEMICAL EVALUATION	43

3.5.1 Radiant Heater Evaluation	43
3.5.2 Heat Flux Data	45
3.5.3 Transient Mass Loss Data	47
3.5.4 Wildfire Chemicals Performance	48
3.5.5 Statistical Analysis	50
4. THERMAL CANISTER DEVELOPMENT	53
4.1 THERMAL CANISTER FABRICATION AND OPERATION	53
4.2 THERMAL CANISTER MATHEMATICAL MODEL	56
4.2 ESTIMATION OF LOSSES	66
4.2.1 Radiation Losses	66
4.2.2 Combustion Exit Losses	67
4.2.3 Total Heat Release Rate	69
5. CONCLUSIONS	72
6. RECOMMENDATIONS FOR FUTURE WORK.....	74
7. REFERENCES.....	76
8. APPENDIX.....	85

LIST OF FIGURES

Figure 2-1:	Drawing of the modified sensor block (all dimensions in mm).....	17
Figure 2-2:	Thermocouple arrangement (a) in the sensor of Sullivan and McDonald [26] and (b) to measure the differential temperature.....	18
Figure 2-3:	Radiant heater panel wiring diagram.....	20
Figure 2-4:	Radiant heater test apparatus (dimensions shown are in meters).....	21
Figure 2-5:	Mass loss cone test apparatus.....	23
Figure 2-6:	Crown fire sensor and logger placement.....	24
Figure 2-7:	Crown fire plot layout.....	25
Figure 2-8:	Radiant heater test skid assembly for wildland fire chemical evaluation.....	26
Figure 2-9:	Burn test during combustion (Flaming of vegetative sample after ignition.....	28
Figure 3-1:	Incident heat flux curves from the radiant heater tests for stand-off distance of (a) 0.102 m and (b) 0.152 m.....	29
Figure 3-2:	View factor for aligned parallel rectangles [57].....	31
Figure 3-3:	Incident heat flux curve from the mass loss cone tests at 40 kW/m ² over (a) short, abrupt time periods and (b) an extended time period.....	36
Figure 3-4:	Incident heat flux curve from the mass loss cone tests at 15 kW/m ² over an extended period.....	38
Figure 3-5:	Transient incident heat flux curve from the controlled crown fire.....	39
Figure 3-6:	Images of the heat flux sensors under extreme crown fire conditions (a) flame front approach, (b) sensors fully engulfed in flames, (c) after the flame passes the sensors.....	40

Figure 3-7:	Relationship between the heat flux at the stand-off distance and the radiant heater surface temperature.....	43
Figure 3-8:	Mean ignition time of an untreated vegetative fuel sample from transient heat flux data (original heat flux sensor by Sullivan and McDonald).....	44
Figure 3-9:	Mean ignition time of an untreated vegetative fuel sample from transient heat flux data (modified heat flux sensor).....	45
Figure 3-10:	Mean ignition time of an untreated vegetative fuel sample from transient mass data.....	46
Figure 4-1:	Representation of the thermal canister walls.....	70
Figure 4-2:	(a) Thermal canister configuration, (b) exploded view of the thermal canister....	71
Figure 4-3:	(a) Representation of the thermal canister wall showing line of symmetry, (b) schematic for the mathematical model.....	53
Figure 4-4:	The absorption and reflection of incident radiation and emitted radiation of the thermal cube sensor [26].....	63
Figure 4-5:	Control volume of the energy through the exhaust pipe	64
Figure 4-6:	Predicted results from the thermal canister model vs the thermal cube model....	77

LIST OF TABLES

Table 3-1:	Properties of air at film temperature [60].....	33
Table 3-2:	Data values from the mass loss cone test for calculation of error values.....	41
Table 3-3:	Comparison of average flaming ignition time from the heat flux and mass loss data.....	47
Table 3-4:	Results from the burn tests for the different wildfire chemicals.....	48
Table 3-5:	<i>t</i> -test results of the average (mean) flaming ignition times through comparison of the wildfire chemicals.....	50
Table 4-1:	Aluminum 6061 material properties.....	73

NOMENCLATURE

A_c	cross-sectional area, m ²
A_s	surface area, m ²
Bi	Biot number
c_p	specific heat at constant pressure, J/kg K
d	sensor depth, m
E	electric potential, V
F_{ij}	radiation view factor
g	gravitational acceleration, m/s ²
H	sensor height, m
h	convection heat transfer coefficient, W/m ² K
k	thermal conductivity, W/m K
L	length, m
m	mass flow rate, kg/s
Pr	Prandtl number
p	pressure, N/m ²
q'	heat transfer rate, W
q''	heat flux, W/m ²
Ra	Rayleigh number
T	temperature, °C
t	time, s
V	fluid velocity, m/s

W thermal canister plate thickness, m
 x, y, z rectangular coordinates, m

Greek Symbols

α thermal diffusivity (m^2/s)

β compressibility factor (K^{-1})

δ half thickness (m)

ε emissivity

λ separation constant (m^{-1})

μ mean time (s)

σ Stefan-Boltzmann constant, $5.67 \times 10^{-8} \text{ W/m}^2\text{K}^4$

τ function dependent on t , only

ν kinematic viscosity (m^2/s)

ρ density (kg/m^3)

Φ function dependent on x , only

Ψ function dependent on x and t

ω error variable

1. INTRODUCTION

1.1 WILDLAND FIRES

Wildland fires have been a common occurrence throughout history and they ultimately play a vital role in the shaping of forest ecosystems [1]. However, there has been a significant increase in wildland fire activity in recent years, resulting in detrimental effects [2]. According to Wang, et al. [3], weather and climate, including temperature, precipitation, wind and atmospheric moisture are critical factors of fire activity. There have been numerous studies that suggest that the temperature is the most important factor affecting overall wildland fire activity, with warmer temperatures leading to increased fire activity [2-5]. This increasing trend of wildland fire activity is expected to continue under plausible climate change scenarios, implying a further increase in the risk of large wildland fires that cause significant damage [2-5].

Over the past three to four decades, wildland fires across Canada have consumed, on average, 2 million hectares each year [6]. Studies have shown that lightning accounts for 35% of Canada's wildland fires; however, these fires result in 85% of the total area burned [7]. These lightning-caused fires often occur in remote areas where human life and property values are not threatened. Therefore, fire suppression in these areas may be intentionally limited; leaving fire to play its natural role with the end result that lightning fires generally grow larger, as detection and subsequent initial attack is often delayed [7]. Human-caused fires, on the other hand, represent the majority of ignition sources [7]. Due to the location of occurrence of these human-caused fires, they are usually detected early and can be accessed quickly by firefighting crews. Still, the threat they pose to human safety and property makes them a major concern. In Canada, fire

agencies spend an average of CAD \$500 million annually on fire management and these expenditures have been increasing due to more active fire occurrences and extreme fire weather conditions in recent years and the projected near future. In addition, as residential areas expand into relatively untouched wildlands (called the “wildland-urban interface”), the threat to the human population by fires is dramatically increased [6, 8-9].

Given the growing concerns regarding increased wildland fire activity, balancing the potential benefits and consequences becomes a complicated, and at times, daunting task, but one that is vital to public safety and the sustainable management of forests and wildlands [10]. Therefore, it becomes necessary to understand further this complex phenomenon of wildland fires and its effects on the surroundings. This will ultimately result in the development of advanced fire management and suppression methods, improved fire codes and strategies, and the more accurate prediction and assessment of fire effects.

1.2 WILDLAND FIRE FUEL CHARACTERISTICS

Another important factor that contributes to the occurrence and magnitude of wildland fire are the forest vegetative fuels. Fuel types, continuity, structure, moisture, and amount are critical factors that influence wildland fire behavior [11]. The different types of wildland fires are characterized as being ground, surface, or crown fires [12]. As outlined by Scott and Reinhardt [12], a ground fire is one that burns in ground fuels such as duff, organic soils, roots, and rotten buried logs. Ground fires burn with very low spread rates, but can be sustained at relatively high moisture contents with high fuel consumption, causing significant damage to trees and shrubs. Although ground fuels can be ignited directly, they are commonly ignited by a passing surface

fire. A surface fire is one that burns in the surface fuel layer, which lies immediately above the ground fuels but below the canopy, or aerial fuels. Surface fuels consist of needles, leaves, grass, dead and down branch wood and logs, shrubs, low brush, and short trees. Surface fire behavior varies widely depending on the nature of the surface fuel complex. A crown fire is one that burns in the elevated canopy fuels. Canopy fuels normally consumed in crown fires consist of the live and dead foliage, lichen, and fine live and dead branch wood found in a forest canopy. Crown fires are usually associated with extreme fire behavior, implying an increase in the rate of spread, intensity, flame length, and spotting [12].

The ignition process for these forest vegetative fuels, as outlined by Holton, et al. [13], occurs in several stages. During the pre-ignition phase, the fuel is heated and its temperature rises toward the ignition temperature (about 390°C for fuels composed mainly of cellulose); so, the ignitability depends on the fuel's initial temperature, as well as its thermal properties. This ignition temperature is typically above the boiling point of water. Therefore, all the moisture present in the fuel must vaporize before ignition occurs. At higher temperatures (200-340°C), the fuel undergoes pyrolysis, which is the thermal decomposition of the fuel to an envelope of flammable gases, semi-volatile tar, and a solid char. Ignition is the transition from pre-ignition to combustion, at a temperature at which external heating is no longer required. Once ignition has been achieved, the heat generated by combustion brings other fuels to ignition, and continues the process. However, combustion may not always involve a flame. After flaming combustion has consumed most of the volatile substances, the remaining solid carbon may burn by smoldering (surface oxidation, also called glowing combustion).

The ignition of wildland fuels generate substantial amounts of energy that are transferred to the surroundings during the combustion process, and the amount of that energy depends on the

conditions that are present. The result of this energy release poses significant threat to the entire surroundings as evident from the destructive nature of wildland fires.

1.3 MEASURING ENERGY TRANSFER IN WILDLAND FIRES

Given the potential impact of wildland fires, understanding the energy transfer during wildland fires is essential for the advancement of wildfire science. Advanced understanding of the energy transfer remains relatively under-developed and poorly documented, partially due to the limitations and shortfalls of the availability of measuring devices for wildland fires [14].

The most common method to measure the intensity of wildland fires is to use Byram's fireline intensity [15]. Byram's fireline intensity is the rate of heat release per unit time per unit length of fire front, and it is measured in kW/m [15]. The fireline intensity represents the radiant or convective energy that is emitted from the flame front and it is an important characteristic for the propagation of a fire, and thus provides critical information for fire suppression activities. It has also been incorporated into fire danger rating calculations [16-19]. Although fireline intensity is a good indication of fire behavior, it can be misleading because it does not correlate to the exact energy that may be emitted from the fire to the surroundings. Therefore, using other techniques to measure the energy release rates and transfer in terms of heat flux (in kW/m²) may be more useful to scientists. Heat flux is the rate at which energy is transferred, by conduction, convection, or radiation, per unit area perpendicular to the direction of that transfer. For example, measuring heat flux, instead of the fireline intensity, provides a single number that can be measured with devices such as a mass loss cone calorimeter for the testing of materials or products [20]. In addition, fire scientists can use heat flux data and directly correlate it to the type

of burn a person could receive [20-21]. For this reason, fireline intensity is not as useful as heat flux because it is difficult to relate fireline intensity to the specific amount of energy to which an object will be exposed [20].

Some commercially available devices for measuring heat fluxes include Schmidt-Boelter gauges, Gardon gauges (also known as a circular-foil gauge), and thin-film thermopiles [22-24]. These commercial sensors are relatively expensive and may be easily damaged when exposed to conditions that are typical during wildland forest fires [25]. Therefore, there is value in developing an inexpensive, robust, and accurate heat flux measurement device to withstand repeated high heat load exposure in extreme fire conditions. Several alternative devices, such as the directional flame thermometer and the hemispherical heat flux gauge, have been developed over the years to measure heat flux in fire conditions [26-28]. However, these alternative devices were not without fault, and it was identified that there were various issues such as inconsistencies in the heat flux estimates and slow response times [26-28].

To resolve some of these adverse issues, Sullivan and McDonald [20] developed a robust and inexpensive custom-fabricated sensor that was capable of measuring high heat loads in wildland forest fire scenarios for extended periods of time, without the use of external cooling. The sensor performed well in both controlled laboratory tests and simulated forest fire tests, estimating the total heat flux within one standard deviation of the values measured by a commercial Schmidt-Boelter heat flux gauge and within an acceptable response time of 8 seconds over an extended time period (typically greater than 10 minutes) [20]. A shortcoming of the sensor was that there were large errors in the measurements of heat flux that were on the order of 110% at low heat flux measurements (order of 13 kW/m² or less), but still significant, errors of 54% at high heat flux measurements (order of 43 kW/m² or higher). There can be value added if a method can be

conceptualized to reduce the large errors in measurements from the heat flux sensor developed by Sullivan and McDonald.

1.4 WILDFIRE SUPPRESSION CHEMICALS

Fire agencies worldwide apply millions of liters of fire suppression chemicals in an attempt to contain and extinguish wildland fires. These chemicals have been proven to be effective firefighting tools for inhibiting the spread and reducing the intensity of wildland fires [29]. The chemicals can mitigate fires directly, through treatment of the burning fuels, or indirectly, in advance of a fire front to create control-lines (a constructed or natural fire barrier) or to reinforce constructed fire-lines (the part of a control line that is scraped or dug to mineral soil) in the unburnt fuel [29]. Fire suppression chemicals include long-term fire retardants, which inhibit combustion, even after vaporization of their water-based matrix, water enhancers, which lose their effectiveness after evaporation of their water content, firefighting foams, which form small bubbles when mixed with water, and wetting agents, which reduce the surface tension of water and increase its ability to spread and wet the fuel surfaces [29-30].

There are many different experimental and analytical methods available that have been used to evaluate the performance of wildfire chemicals, such as gas chromatography, Fourier transform infrared spectroscopy, mass spectrometry, and thermal gravimetric analysis [30-35]. However, Wang, et al. [35] have shown that the small test samples used and the rapid removal of pyrolysis or combustion products can result in erroneous interpretations of the resulting data in terms of forest fuel flammability in real situations [30]. Therefore, the information provided by analytical methods should be supported by other laboratory-scale fire tests. There are a few laboratory-

scale tests applicable for evaluating wildfire chemicals. Liodakis, et al. [30] successfully developed one such laboratory test and apparatus to determine the influence of retardants on the flammability parameters of forest vegetation species. In the wildfire industry, the ASTM E1321-13 [36] Standard Test Method for Determining Material Ignition and Flame Spread Properties is widely accepted as the laboratory test method of choice for wildfire chemicals. The US Forest Service uses this standard to develop the Evaluation of Wildfire Chemicals Test Procedure [37]. These tests, however, do not use actual vegetative samples to provide an indication of field performance where, instead, a plywood substrate is used for evaluation [37].

Based on a review of several published studies, ignition tests are considered the most suitable for the differentiation of wildfire chemicals. There have been numerous experimental ignition studies conducted on various materials [38-41]. In relation to studies of wildfire chemicals, Tafreshi and Di Marzo [38] conducted ignition studies on gel- and foam-treated samples to determine their effectiveness as fire retardants. However, as with much of the ignition studies on fire chemicals, the tests were typically done on non-foliar vegetative samples and if so, the samples were relatively small and could not provide a true representation of a real fire scenario. It was also noted that the time-to-ignition data obtained in these studies were primarily based on visual measurements. However, there may be cases where visual measurements may prove to be onerous and prohibitive. For example, determining the time-to-ignition visually in flash fires may prove to be onerous, from a health and safety point of view, due to the high fluxes generated (heat fluxes of approximately 84 kW/m^2 according to NFPA 2113 [42]) and the spontaneous nature of the ignitions (which lasts for approximately 3 s according to NFPA 2113 [42]). Similar problems are also encountered in enclosed fires (such as building fires and controlled large-scale wildfires) and also fuel oil-based fires.

There are a variety of measurement apparatus available on the market that can be used to quantify the performance and energy release rates from chemically treated vegetative samples. One such apparatus is the mass loss cone calorimeter, a common bench-scale apparatus that uses oxygen consumption to estimate heat release rates, which has been used for fire retardancy measurements on wood products [43]. This device has been used to measure energy release rates of ignited solid and thick materials such as building materials, plastics, and wood products, rather than foliar (vegetative) samples [43-46]. Further issues also arise in terms of the portability of the mass loss cone calorimeter if tests are required to be conducted in an isolated area or field location.

A device that has been constantly overlooked for evaluating wildfire chemicals is the portable heat flux sensor. Heat flux sensors are used to quantify the energy transfer during high heat load applications and may have some merit as an essential tool in evaluating the effectiveness of wildfire chemicals. Therefore, there is a case for utilizing heat flux sensors in the development of an effective methodology to differentiate wildfire chemicals using foliar (vegetative) samples to provide an indication of the potential performance in a real fire scenario. Comparison of the performance of various types of suppression chemicals will aid in strategic planning for combatting wildland fires as well as reduce the immense costs necessary to contain them. In the forestry industry, the US Forest Service provides a comparison of the different wildfire chemicals based on their time-to-ignition [47-49].

1.5 FIRE CALORIMETRY

The heat flux sensor was suggested as a potential tool for evaluating the performance of wildfire chemicals in Section 1.4. The sensor would be used to determine the time-to-ignition of a sample

treated with wildland fire chemical, based on the incident heat flux from the combustion process. The estimated time-to-ignition provides valuable information regarding the relative performance of wildfire chemicals. However, the incident heat flux data by itself would not be considered a useful quantity for the purposes of evaluating the relative performance of the wildfire chemicals. From the combustion process, the incident heat flux may vary based on the orientation and position of the heat flux sensor relative to the burning sample. Based on the design of the custom-built thermocouple-based heat flux sensor developed by Sullivan and McDonald [20], it may be possible to develop a suitable method to measure the total heat release rate from the combustion process, and which takes advantage of the heat flux data. According to Janssens [50], the heat release rate is regarded as one of the most significant properties for understanding the combustion process and fire characteristics, which can be used for evaluating the performance of various products. There have been numerous methods that have been developed for determining the heat release rate [50]. However, the methods for determining the heat release rate are based fundamentally on measurements of oxygen consumption and sensible enthalpy rise [50].

The oxygen consumption method is the most commonly used method for determining the heat release rate [50]. The heat release rate is determined from the oxygen concentration and the flow rate of exhaust products. Thornton [51] observed that a constant net amount of heat is released per unit mass of oxygen consumed for complete combustion. As outlined by Janssens [50], the basic requirement to use the oxygen consumption technique is that all of the combustion products are collected and removed through an exhaust duct. At a distance downstream that is sufficient for adequate mixing, both flow rate and composition of the gases are measured. The heat release rate, q'_{oc} from the oxygen consumption principle can be expressed as [50]:

$$q'_{oc} = E_{O_2} (\dot{m}_a Y_{O_2}^a - \dot{m}_e Y_{O_2}^e), \quad (1-1)$$

where E is the heat release per unit mass of oxygen consumed, \dot{m}_a is the mass flow rate of the inlet air, \dot{m}_e is the mass flow rate of the combustion products, $Y_{O_2}^a$ is the mass fraction of oxygen in the combustion dry air, and $Y_{O_2}^e$ is the mass fraction of oxygen in the combustion products. According to Janssens [50], the practical implementation of the oxygen consumption method is not straightforward. Oxygen analyzers measure the mole fraction and not the mass fraction of oxygen in a gas sample [50]. Also, flow meters measure volumetric flow rates, rather than mass flow rates [50]. The volumetric flow rate in the exhaust duct, normalized to the same pressure and temperature, is usually slightly different from the inflow rate of air because of expansion due to the combustion reactions [50]. Equations were later developed for calculating the rate of heat release by oxygen consumption for various applications, as presented by Janssens [50]. The equations are not repeated here, and can be found in the aforementioned study [50]. The differences in treatment and equations to be used are mainly due to the extent to which gas analysis is made [50]. As a minimum, the oxygen concentration must be measured. However, accuracy can be improved by adding instrumentation for measuring the concentration of CO₂, CO and H₂O [50].

The oxygen consumption technique is the most accurate and convenient way to measure the heat release rate from fires [50]. Disadvantages of the technique are the high cost of instrumentation (only oxygen analyzers of the highest quality and precision are adequate), and the need for a rigorous calibration and maintenance schedule [50]. The heat release rate can also be measured on the basis of the carbon dioxide that is generated. The advantage of this technique is that it is easier and less costly to measure carbon dioxide with sufficient accuracy, than it is to measure

oxygen [50]. However, the amount of energy generated per unit mass of carbon dioxide generated is much more fuel-dependent than the amount of energy produced per unit mass of oxygen consumed [50]. To develop a suitable method for measuring the heat release rate, while trying to utilize the concept of the heat flux sensor, based on the oxygen consumption would not be practical given the high level of complexity and the high associated costs. Therefore, the method of sensible enthalpy rise was explored [50-51].

The sensible enthalpy rise method was the first to be used in fire calorimetry due to its simplicity; it is still in use today [50]. The heat release rate is measured on the basis of the difference in temperature between the air supplied at a constant rate to the combustion chamber, and the products of combustion [50]. The sensible enthalpy method is based on the following equation [50]:

$$q' - q'_{fl} = \dot{m}_a c_p (T_e - T_a), \quad (1-2)$$

where q' is the heat release rate, q'_{fl} is the rate of heat loss, \dot{m}_a is the mass flow rate of the entrance air, c_p is the average specific heat of air, T_e is the temperature of the combustion products leaving the control volume, and T_a is the temperature of the air entering the combustion zone. The heat release rate is calculated from the temperature rise ($T_e - T_a$) of the gases flowing through a calorimeter. As outlined by Janssens [50], calorimeters based on the sensible enthalpy rise method use a closed configuration. The specimen and heater are located inside a metal box, which may be insulated, either completely or in part. By monitoring the temperature change of the walls surrounding the combustion gases, the total heat released by a sample can be determined in terms of heat balances on and within the total system. The dynamic response of the enclosure to changes in the thermal environment creates major impediments to the practical

implementation of the sensible enthalpy rise method. After ignition, some of the heat released by a burning sample is transferred by radiation to the enclosure walls. A fraction of this heat is stored in the walls, causing an increase of its temperature, in turn resulting in enhanced heat transfer with the air flowing through the box. The result is that, for a material that quickly reaches steady burning conditions, there is a delay for T_e to reach the corresponding steady temperature. A similar phenomenon occurs when heat release rate from the specimen decreases, or after the specimen burns completely and the heat release rate returns to zero. Under unsteady burning conditions, T_e lags behind the temperature corresponding to the instantaneous heat release rate [50]. If high accuracy is not critical, the sensible enthalpy rise method can be used because of its simplicity and the simple instrumentation that is needed. However, it is difficult to eliminate dynamic errors associated with thermal lag [50].

Given the simplicity and low cost, the sensible enthalpy rise method could be considered an appropriate method to emulate to measure the heat release rate with a thermocouple-based sensor design. The method is based on monitoring the temperature change of the combustion chamber walls surrounding the combustion gases and the total heat released is determined in terms of heat balances on and within the total system. This can be adopted by developing a combustion chamber that is essentially a series of thermocouple-based heat flux sensors, where the incident heat flux measurements can be converted to heat flow rate. An energy balance can then be performed similar to the sensible enthalpy method to determine the total heat release rate.

1.6 OBJECTIVES

The overall objectives of this study were to:

1. Determine a suitable method for reducing the large errors in the custom thermocouple-based heat flux sensor that was developed by Sullivan and McDonald.
2. Validate the performance of the improved heat flux sensor by:
 - i. Testing the sensor in a controlled laboratory environment to validate the sensor and model.
 - ii. Testing the sensor in a simulated forest fire environment.
 - iii. Comparing the heat flux results with data obtained from the original heat flux sensor and a Schmidt-Boelter gauge, which is a well-documented and calibrated commercial sensor.
3. Develop an effective test method to differentiate wildfire chemicals, utilizing the custom thermocouple-based heat flux sensor.
4. Develop a mathematical model for a custom-made calorimeter, based on the thermocouple-based heat flux sensor design, which can estimate the total heat release rate from a small-scale combustion process involving vegetative fuels.

1.7 THESIS ORGANIZATION

This thesis document is divided into the following chapters. Chapter 2 describes the experimental method used to improve and validate the design of the custom thermocouple-based heat flux sensor. The experimental method for using the improved heat flux sensor design in the application of evaluating the performance of wildfire chemicals (water, foam, gels, and long-term retardant) is also presented. Chapter 3 presents the results and analysis of the validation tests for the improved heat flux sensor. The results and analysis from evaluation of wildland fire chemical are also presented. Chapter 4 describes the mathematical model that couples with the thermal calorimeter that is used to estimate the total heat release rate from the combustion of vegetative fuel. The fabrication and operation of the thermal calorimeter is also presented. Chapter 5 presents the conclusions of this study, and Chapter 6 discusses the possible future work that may be extended from this thesis study.

2. MATHEMATICAL MODELS AND EXPERIMENTAL METHODS

2.1 HEAT FLUX SENSOR DEVELOPMENT

The custom heat flux sensor that was developed by Sullivan and McDonald [20] was based on using experimentally measured temperature data as input parameters into a heat conduction model, idealized as a one-dimensional, finite-length scale problem, for the incident heat flux on the surface of the sensor. Equation (2-1) shows the developed heat flux model, that was corrected for the radiation reflected from the surface and the radiation emitted from the sensor as it increases in temperature [20]

$$q''_{\text{incident}}(t) = \frac{1}{\varepsilon} \left(\frac{k[T(d,t) - T_1(t)]}{(L-d)} + \sigma \varepsilon [T(d,t)^4 + T_1(t)^4 - 2T_\infty^4] \right) \quad (2-1)$$

where, q''_{incident} is the incident heat flux in the surface of the sensor, t is time, k is the thermal conductivity of the sensor material, ε is emissivity, σ is the Stefan-Boltzmann constant ($5.67 \times 10^{-8} \text{ W/m}^2\text{-K}^4$), L is the thickness of the sensor, d is the depth into the sensor where a thermocouple is located, T_∞ is the surrounding ambient temperature, $T_1(t)$ is the backside temperature, and $T(d,t)$ is the temperature at location d in the sensor.

An uncertainty analysis was conducted by Sullivan [52] on Eq. (2-1) to determine the error in the incident heat flux from the heat source. There are eight variables, namely, ε , k , σ , T_∞ , $T(d,t)$, $T_1(t)$, L , and d in Eq. (2-1), which may have uncertainty that affects the accuracy of the incident heat

flux estimate. The propagation of uncertainties in the estimations of the heat flux was determined by Sullivan [52] using Eq. (2-2), as derived by Taylor [53].

$$\begin{aligned} \left(\frac{\omega_{q_{net}}}{q_{net}} \right)^2 &= \left(\frac{[(\omega_{T_1(t)})^2 + (\omega_{T(d,t)})^2]^{1/2}}{T_1(t) - T(d,t)} \right)^2 + \left(\frac{[(\omega_L)^2 + (\omega_d)^2]^{1/2}}{(L-d)} \right)^2 \\ &+ 8 \left(\frac{\omega_{T_1(t)}}{T_1(t)} \right)^2 + 8 \left(\frac{\omega_{T(d,t)}}{T(d,t)} \right)^2 \end{aligned} \quad (2-2)$$

The analysis indicated that the sensor produced very large errors of 110% at low heat flux measurements (13 kW/m² or less) and lesser, but still significant, errors of 54% at high heat flux measurements (43 kW/m² or higher). The inherent thermocouple errors of 1.1°C, based on the manufacturer's limit of error, for each temperature measurement was identified as a significant contributor to these large errors. It should be noted that the actual thermocouple error may in fact be less than 1.1°C, as this stated value represents an estimate of the limit of error for the entire batch of thermocouples manufactured; however the worst case scenario was used for the analysis. Based on the most conservative scenario, this poses a serious problem when measuring the small temperature differences that occur within the sensor [20]. In order to reduce these large errors, more focus was therefore given to temperature measurements.

The large errors in the heat flux estimates, caused by the inherent errors in the thermocouple readings of temperature, can be mitigated if the differential temperature is measured directly instead of the absolute temperature of the back and front side of the sensor as was done by Sullivan and McDonald [20] and Sullivan [52]. Measuring the temperature difference, rather than the absolute temperature values, will reduce these large errors since the propagation of the inherent thermocouple errors will be reduced, as is evident from the first term in Eq. (2-2). To

that end, the heat flux model that was developed by Sullivan and McDonald [20] was modified to use experimentally measured differential temperatures. In this study, the measured temperature differential was represented as

$$\Delta T = T(d, t) - T_1(t) \quad (2-3)$$

Therefore, Eq. (2-1) was modified to become,

$$q''_{\text{incident}}(t) = \frac{1}{\varepsilon} \left(\frac{k\Delta T}{(L-d)} + \sigma\varepsilon \left[T(d, t)^4 + T_1(t)^4 - 2T_\infty^4 \right] \right) \quad (2-4)$$

The temperature difference was measured in terms of the induced voltage produced in order to negate the reference junction (cold junction) compensation. The voltage difference that was produced was converted to a temperature difference by using an established scale based on a reduced order approximation of the quartic form from the IPTS-68 (International Practical Temperature Scale) [54]. The reduced order approximation is given in Eq. (2-5) as

$$\Delta T = a_0 + a_1 E^2 + a_2 E^3 + a_3 E^4 \quad (2-5)$$

where E is the voltage in millivolts, and a_n is the approximation coefficient obtained from calibration data [54].

2.2 MODIFIED HEAT FLUX SENSOR DESIGN AND FABRICATION

The modified heat flux sensor was similar in design to that which was developed by Sullivan and McDonald (The Thermal Cube) [20], and was a 50.8 mm x 63.5 mm x 25.4 mm (2 in x 2.5 in x 1 in) rectangular block of 6063-T6 aluminum, with thermocouples inserted for temperature

measurement as shown in Fig. 2-1. The front and back side of the block was painted with a high-temperature black spray paint (Krylon 1618 BBQ and Stove Paint, The Sherwin-Williams Company, Cleveland, OH, USA) to increase the emissivity so that it approached that of an ideal black-body and to enhance absorption of almost all radiation heat transfer. The key modification to the design was that an additional 2 mm (0.08 in) diameter hole that was drilled adjacent to the 2 mm (0.08 in) hole at the front of the sensor. A thermocouple was inserted in the additional hole in order to measure the absolute temperature at the front side.

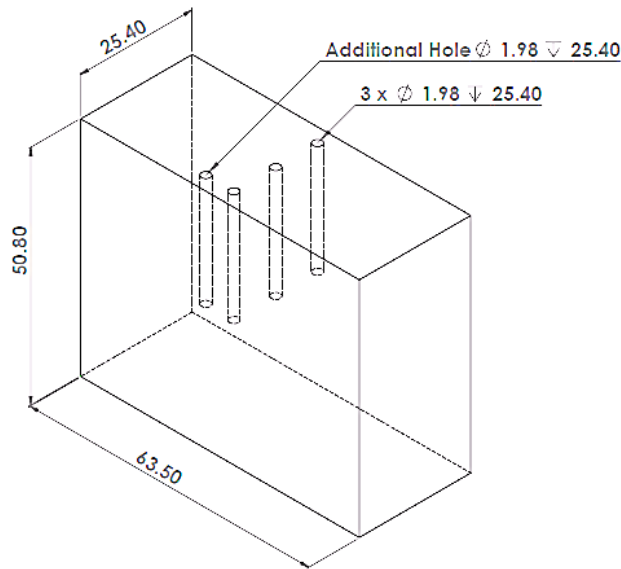


Figure 2-1: Drawing of the modified sensor block (all dimension in mm).

The thermocouple arrangement in the sensor of Sullivan and McDonald [20] is shown schematically in Fig. 2-2(a). The thermocouples were used to measure the backside and the front side temperatures of sensor. Type-J, 30 gauge thermocouples (Iron-Constantan) (Omega Engineering, Inc., Laval, QC, Canada) were selected due to their ability to measure temperatures over a broad temperature range (-210 to 750°C), high sensitivity (51 $\mu\text{V}/^\circ\text{C}$), and low cost. The sides of the sensor were then insulated by using M-board insulation (M-board, Industrial

Insulation Group, Augusta, GA, USA) in order to drive a one-dimensional transfer of energy through the sensor.

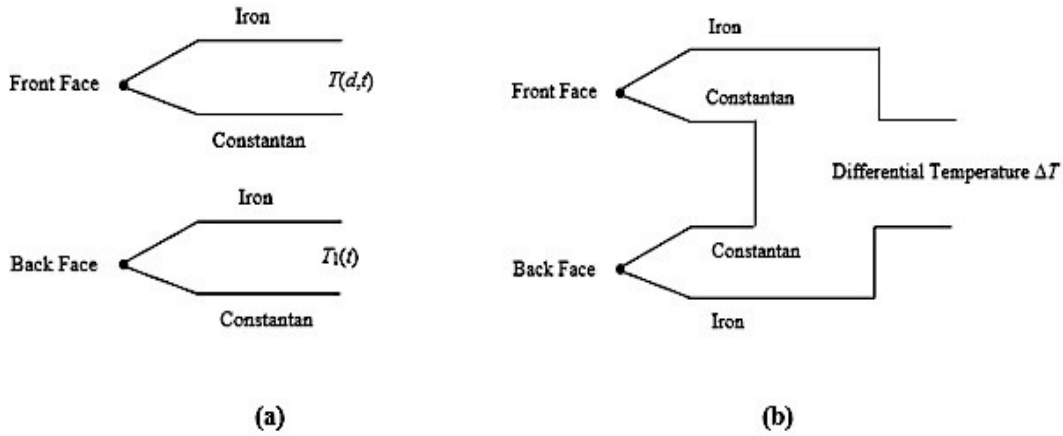


Figure 2-2: Thermocouple arrangement (a) in the sensor of Sullivan and McDonald and (b) to measure the differential temperature

The arrangement to measure the differential temperature for the modified sensor is shown in Fig. 2-2(b). To obtain the differential temperature, the two identical metals (constantan) of the thermocouples were joined together while the two iron wires were fixed to the thermocouple connector. The voltage generated between the two iron wires corresponded to the temperature difference between the two thermocouple junctions, which represented the differential temperature that was measured.

2.3 MODIFIED HEAT FLUX SENSOR VALIDATION

The objective of the validation tests was to provide heat flux data for testing the performance of the modified heat flux sensor using differential temperature measurements. To accomplish this, transient heat flux tests, constant heat flux tests, and controlled field tests were conducted by using an electric-powered radiant heater (Omegalux QH-121260, Omega Engineering, Inc., Laval, QC, Canada), a mass loss cone calorimeter (Mass Loss Calorimeter ISO 13927, Fire Testing Technology, East Grinstead, West Sussex, UK), and a control field plot respectively.

For each test, the results were collected by using a stand-alone data acquisition and analysis system (DaqPRO™ 5300, Fourier Systems Inc., Mokena, IL, USA). The data acquisition system used a 16-bit system with 8 channels for data collection. The temperature measurements were collected at a sampling rate of 1 Hz (1 data point per second) for the thermocouples from the sensors. Also, to establish a benchmark for the tests and to provide data for comparison, a calibrated Schmidt-Boelter gauge (64 series, Medtherm Corporation, Huntsville, AL, USA) was used along with the original heat flux sensor by Sullivan and McDonald [20]. The cooling water flow rate for the Schmidt-Boelter gauge was set to approximately 30 L/hr, with the water supply temperature at approximately 22°C.

2.3.1 Electric Powered Radiant Heater Test

Transient heat flux tests were conducted with a 0.31 m x 0.31 m (12 in x 12 in) electric-powered radiant heater (Omegalux QH-121260, Omega Engineering, Inc., Laval, QC, Canada). The radiant heater was rated at 240 VAC, 1 phase, 1660 – 8640 watts, which allowed for incident heat fluxes of up to 90 kW/m², with a maximum surface temperature rating of up to 980°C. The

heater was connected to a silicon-controlled rectifier (SCR) power controller (SCR39P- 24-040, Omega Engineering, Inc., Laval, QC, Canada), a 1/32 DIN temperature controller (CN7533, Omega Engineering, Inc., Laval, QC, Canada), and an AC current indicator (DP450-HACC, Omega Engineering, Inc., Laval, QC, Canada) to monitor and control the power output, all of which were securely mounted inside a NEMA (National Electrical Manufacturers Association) 13 enclosure located at 2.44 m (8 ft.) from the heater. Figure 2-3 shows a complete wiring diagram of the system.

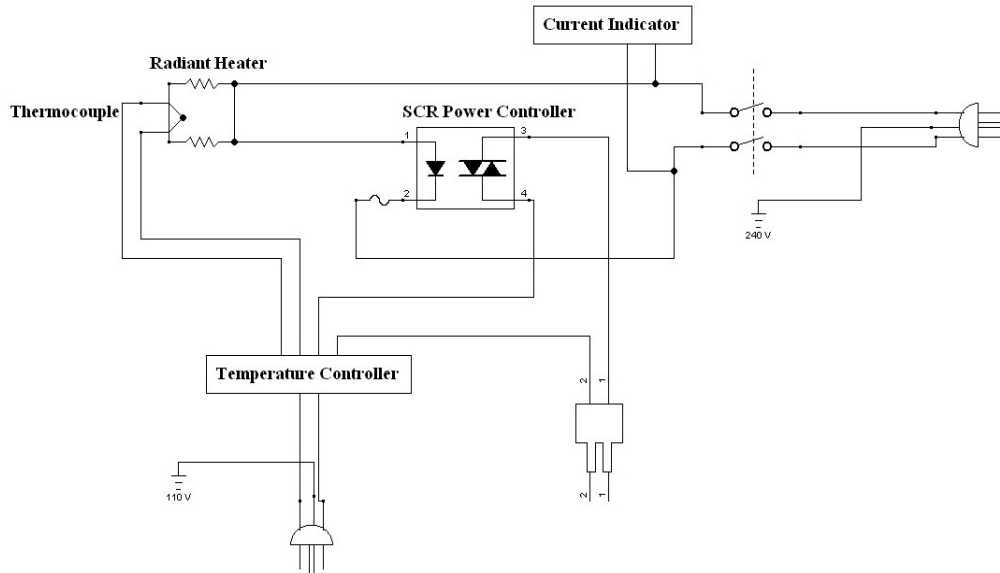


Figure 2-3: Radiant heater panel wiring diagram.

The radiant heater was securely mounted on to a portable skid. The thermal cube was positioned directly in front of the radiant heater (see Fig. 2-4). The thermal cube was clamped on to a sliding plate, capable of moving along the skid to vary the exposure energy as a function of the distance from the radiant heater (the stand-off distance). The stand-off distances used for the tests were 0.102 m (4 in) and 0.152 m (6 in) in order to absorb the maximum possible energy

output safely from the radiant heater. Before each test, the samples were shielded from the heater by using an aluminum sheet until the heater surface temperature was approximately 120°C. Then, the shield was removed to expose the sensor to the thermal load. This shielding process ensured that for each test that was performed, the sensors were consistently exposed to the same initial heat flux of approximately 2 kW/m² at the 0.102 m (4 in) stand-off distance and approximately 4 kW/m² at the 0.152 m (6 in) stand-off distance. The radiant heater was then allowed to heat its surface up from 120°C to 620°C to evaluate the response of the thermal cube to increasing heat flux values. Each test was performed twice to ensure repeatability and the sensor was cooled to within ±10°C of the first test to ensure that the sensor had the same initial temperature for each test.

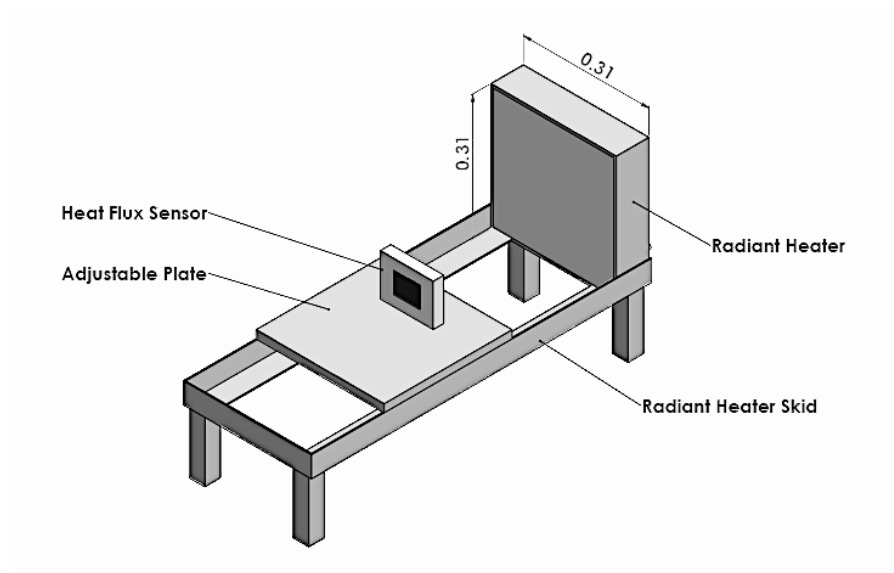


Figure 2-4: Radiant heater test apparatus (dimensions shown are in meters).

2.3.2 Mass Loss Calorimeter Test

By adjusting the temperature settings on the mass loss cone, heat fluxes in the range of those produced by typical wildland fires were used in the simulated tests up to a heat flux of 100 kW/m². For the tests performed in this study, the temperature of the mass loss cone surface was set to 600°C to generate a heat flux of approximately 40 kW/m². This heat flux was selected to accord with the heat fluxes observed by Silvani and Morandini [55]. To evaluate the effectiveness of the sensor at low heat fluxes, the temperature of the mass loss cone was adjusted to 400°C to generate a heat flux of approximately 15 kW/m². The sensors were positioned horizontally at 0.025 m (1 in.) from the edge of the mass loss cone as shown in Fig 2-5. Prior to each test, at 40 kW/m² and 15 kW/m², a calibrated Schmidt-Boelter gauge (64 series, Medtherm Corporation, Huntsville, AL, USA) was used to ensure that the targeted heat flux values were achieved at the set temperature of the mass loss cone.

The heat flux was varied by opening a shutter for two minutes, closing for one minute, and then reopening for another two minutes to evaluate the response of the sensor and demonstrate that the sensor was capable of measuring large, abrupt changes in heat flux, similar to tests conducted by Sullivan and McDonald [20]. Each test was performed twice to ensure repeatability and the sensor was cooled to within ±10°C of the initial temperature condition of the first test. In addition, an extended test was conducted to measure the heat flux, where the shutter was left open for 5 minutes to evaluate the effectiveness of the sensor when exposed to extended periods of low and high heat fluxes. Silvani and Morandini [55] have shown that heat fluxes of burning vegetative fuels ranges from 20 to 80 kW/m², for periods of three to four minutes.

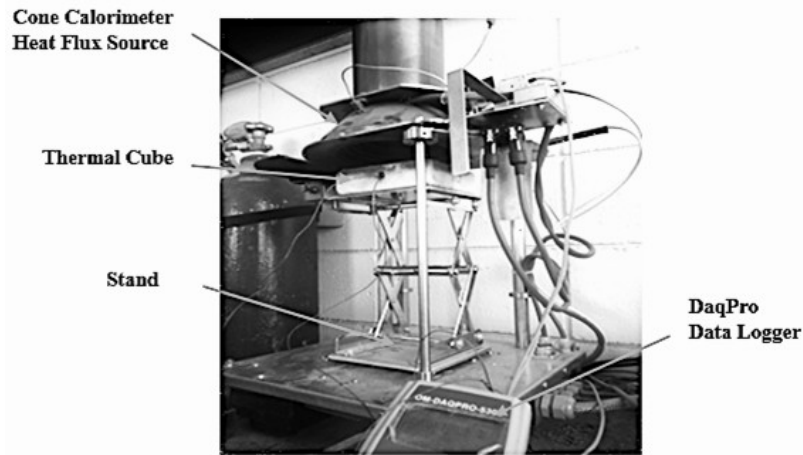


Figure 2-5: Mass loss cone test apparatus

2.3.3 Controlled Crown Fire Test

A controlled crown fire test was conducted at the Canadian Boreal Community FireSmart Project site, North West Territories (located west off highway #3 approximately 40 km north east of Fort Providence) in order to test the capabilities and performance of the sensors in a high heat load field environment. The crown fire was initiated in a selected control plot (approximately 7800 m²) adjacent to Plot # I-3 (See Appendix A), where transient temperature data was collected by using both the original and modified heat flux sensor. The control burn plot consisted of live and dead Jack Pine (*Pinus banksiana*) stands along with various mixed surface fuels accumulated over time.

The heat flux sensors were placed in the ground, mounted on a 1 m pole approximately 6 m from the ignition line with a small hole dug below the sensors that was approximately 50 cm deep in order to bury an 8-channel data logger (DaqPRO™ 5300, Fourier Systems Inc., Mokena, IL, USA), as shown in Fig. 2-6. The logger was buried and wrapped in plastic bags for protection

from the anticipated high intensity crown fire and also from the water used during extinguishing of the fire. The thermocouples in the sensors were then attached to the logger and were set to take a sample every second (1 Hz sampling rate). Both sensors were placed at similar distances from the ignition line for purposes of comparing the collected data. An insulated video camera box was placed 0.91 m (3 ft.) behind the sensors to observe the fire behavior during the crown fire and also how the fire affects the sensors. The plot was then ignited (line ignition) using a MYAC Terra-Torch (MYAC Consulting, Sherwood Park, Alberta, Canada), along the upwind edge of the control plot as shown in Fig. 2-7, and was burnt to completion.

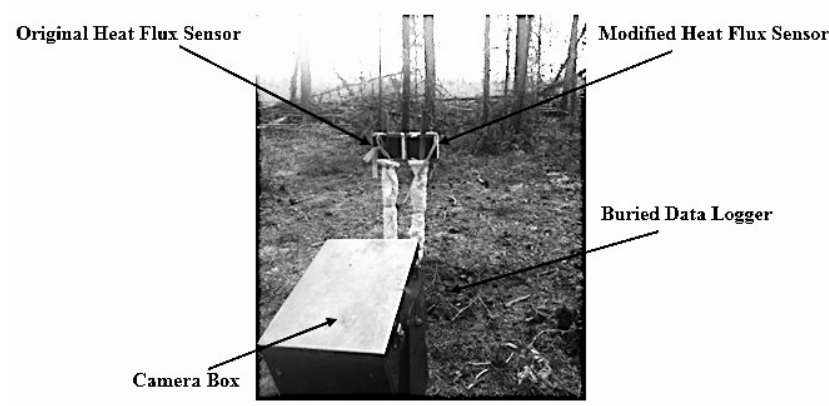


Figure 2-6: Crown fire sensor and logger placement.

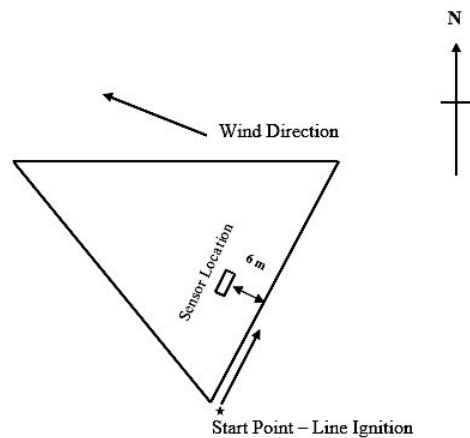


Figure 2-7: Crown fire plot layout.

2.4 EVALUATION OF WILDFIRE CHEMICALS

2.4.1 Wildfire Chemicals Evaluation Apparatus

The same test skid used for the electric-powered radiant heater test (Section 2.3.1) was also utilized to accommodate the test equipment and instrumentation as shown in Fig. 2-8 for the wildfire chemicals evaluation. The radiant heater panel was securely mounted on to the skid in front of the vegetative fuel sample that was in an aluminum mesh cage (see Fig. 2-8). The vegetative fuel sample was mounted on to a calibrated S-Beam type load cell, rated for a maximum mass load of 2 kg (4.4 lbs.). The load cell assembly was moved along the skid to vary the energy incident on the vegetative fuel sample as a function of the distance from the radiant heater (the stand-off distance). The modified custom-built heat flux sensor was positioned directly behind the fuel sample.

For each test, the results were collected by using a stand-alone data acquisition and analysis system (DaqPRO™ 5300, Fourier Systems Inc., Mokena, IL, USA). The data acquisition system used a 16-bit system with 8 channels for data collection. The temperature measurements were collected at a sampling rate of 1 Hz by thermocouples connected to the heat flux sensor, as well as voltage measurements from the load cell.

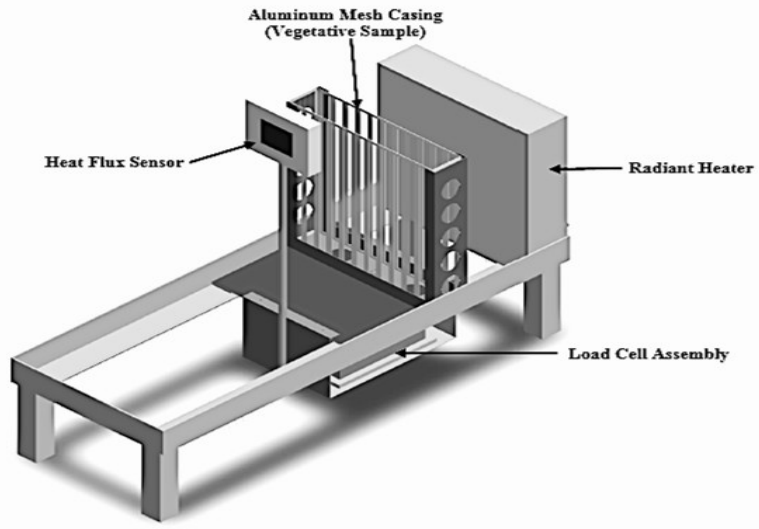


Figure 2-8: Radiant heater test skid assembly for wildland fire chemical evaluation.

2.4.2 Wildland Fire Chemical Evaluation Methodology

The wildland fire chemical products that were used in this study were water, foam, gel, and long-term retardants. The names of these products have been intentionally excluded for proprietary reasons. The concentration of the products chosen was within the range of the mix ratio qualified by the US Forest Service Specifications [47-49]. Lodgepole Pine (*Pinus Contorta*) was the vegetative fuel sample that was used to evaluate the performance of the specified chemical treatments. The pine samples were dried over a 2-month period. The moisture content was measured, in accordance with the ASTM D4442 oven dry standard method [56], before the burn tests were conducted. This was necessary to ensure that a “dry” sample, with less than 5% moisture content, was used to reduce variability in the test results and provide an attainable and repeatable condition of the vegetative fuel material. The vegetative samples, weighing 75 g, were prepared from the pine branches and then sandwiched inside the 0.31 m x 0.31 m x 0.025 m (12 in x 12 in x 1 in) aluminum mesh casing. The wildfire chemicals were applied to the vegetative

fuel samples by dipping the entire aluminum mesh casing into a container containing the suppression chemical. The mesh casing containing the vegetative fuel samples was then mounted on the load cell, which was positioned at a stand-off distance of 0.102 m (4 in) from the radiant heater. Before each test, the samples were shielded from the heater by using an aluminum sheet until the heater surface temperature was approximately 200°C. Then, the shield was removed to expose the sample to the thermal load. This shielding process ensured that for each burn test that was performed, the vegetative fuel samples were consistently exposed to the same initial heat flux of 5 kW/m² at the 0.102 m (4 in) stand-off distance.

Prior to the combustion tests, an evaluation of the performance of the radiant heater was conducted to determine the variation of heat fluxes and temperatures that were experienced by the vegetative fuel sample at the specified standoff distance. The response time of the heater was measured by a Type-J, 30 gauge thermocouple (iron-constantan) (Omega Engineering, Inc., Laval, QC, Canada), from cold start to an operating temperature of 600°C. The heat flux and the temperatures were measured at the specified standoff distance by using a Schmidt-Boelter Gauge (64 series, Medtherm Corporation, Huntsville, AL, USA) and a Type-J, 30 gauge thermocouple (iron-constantan) (Omega Engineering, Inc., Laval, QC, Canada), respectively. The operating temperature of the heater was restricted to 600°C, which is the recommended limit for using the Schmidt-Boelter Gauge without water-cooling. The results from the evaluation that was conducted at the 0.102 m (4 in) standoff distance is shown in Fig. 3-7 (Section 3.5.1).

The time to glowing ignition was determined by visual observation and with a stopwatch. An exhaust fan in the test hood was powered on after the sample started to glow to reduce the accumulation of heavy smoke inside the space. The heat flux data was used to determine the time

to flaming ignition and the transient mass loss data from the load cell was used for verification of that ignition time. Figure 2-9 shows the burn test during combustion of the vegetative sample.



Figure 2-9: Burn test during combustion (flaming of vegetative sample after ignition).

3. RESULTS AND DISCUSSIONS

3.1 ELECTRIC POWERED RADIANT HEATER TEST

The resulting incident heat fluxes that were estimated from the heat flux sensors for one of the representative tests conducted with the radiant heater at the stand-off distances of 0.102 m (4 in) and 0.152 m (6 in) are shown in Fig. 3-1.

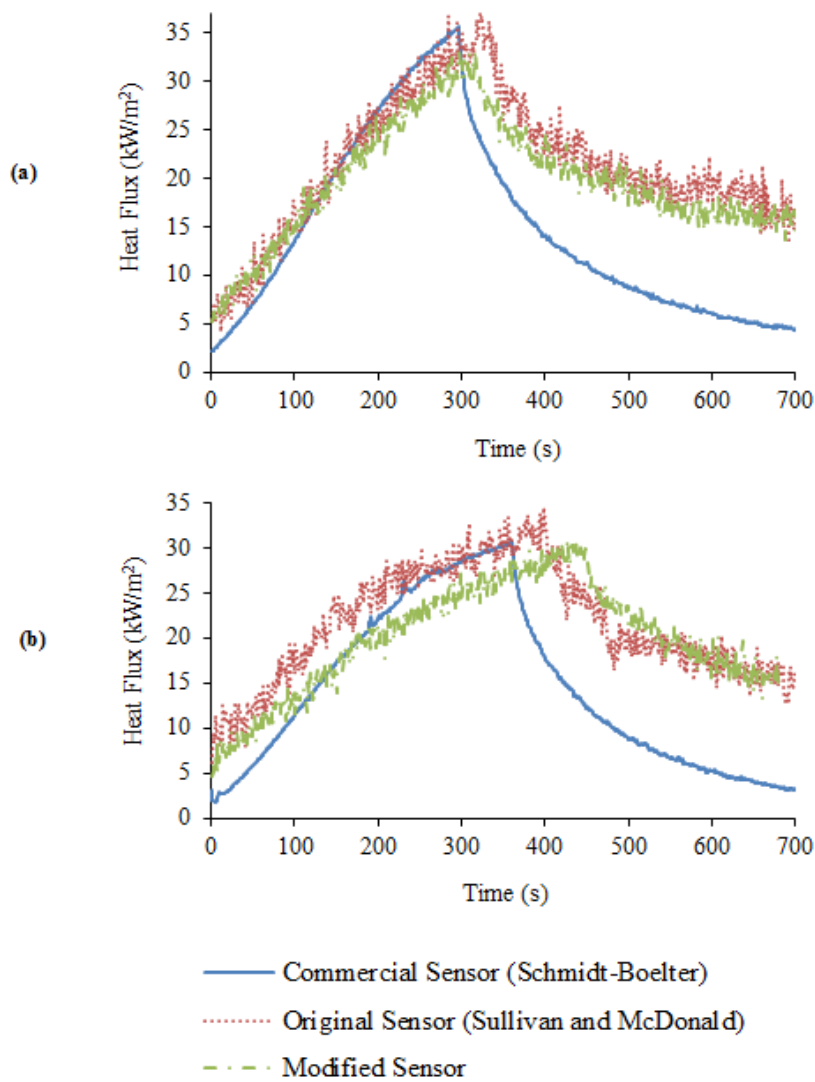


Figure 3-1: Incident heat flux curves from the radiant heater tests for stand-off distance of (a) 0.102m and (b) 0.152m.

Initially, Eqn. 2-1 and Eqn. 2-4 were used to generate data points for the incident heat flux curve, as predicted with temperature data from the original and modified sensor, respectively. It should be highlighted that the initial heat flux was not zero since the initial temperature of the radiant heater was 120°C, which produced approximately 2 kW/m² of heat flux at the 0.102 m stand-off distance and 3 kW/m² at the 0.152 m stand-off distance. There was an observed over-prediction of approximately 3 kW/m² for the initial heat flux estimates from both custom sensors, with eventual agreement with the measurements from the commercial Schmidt-Boelter gauge. This can be attributed to the smaller surface area of the Schmidt-Boelter gauge that resulted in the measurement of a heat flux that was lower than that which was estimated by the custom sensors. When the radiant heater was then powered down, there were further deviations between the measured heat fluxes of the commercial sensor and those of the custom sensors. This was mainly due to the influence of water-cooling that resulted in the rapid removal of heat from the Schmidt-Boelter gauge, while the custom sensors were only air-cooled.

At the 0.102 m stand-off distance, there was a linear variation in the incident heat flux as the temperature of the radiant heater increased. According to the manufacturer [57], by positioning the commercial sensor at 0.0508 m (2 in) from the radiant heater, the sensor was able to absorb up to 80% of the emitted radiant energy from the heater. The percentage of radiant energy leaving the heater that was incident on the heat flux sensors at 0.102 m stand-off distance was determined graphically based on the view factor. The view factor is a function the geometric relationship between the size of the radiant heater and the heat flux sensors and the distance between them, and it determines how much of the radiated energy is incident on the sensors [58]. The radiant heater and heat flux sensor arrangement was assumed to be aligned parallel rectangular surfaces and the view factor was determined graphically from Fig. 3-2 [58].

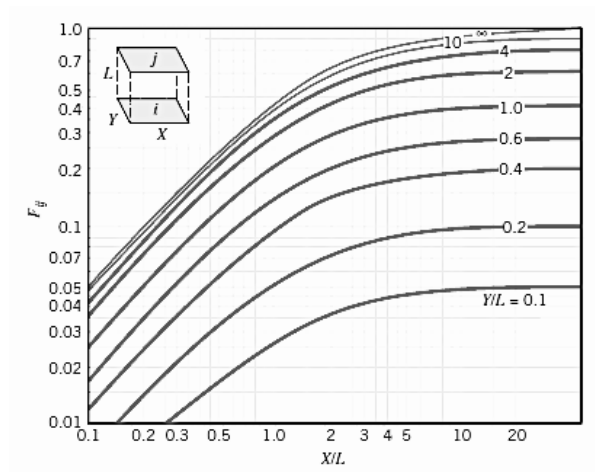


Figure 3-2: View factor for aligned parallel rectangles [58].

Based on Fig. 3-2, the percentage of the radiant energy that was incident on the heat flux sensors was approximately 60% at the stand-off distance 0.102 m. Therefore, the maximum available heat flux at 0.102 was approximately 54 kW/m^2 (based on the heater rated maximum of 90 kW/m^2). The observed noise levels in the estimated incident heat fluxes from the sensors data was due to the combined result of convection at the surface of the sensors and the absence of signal filters. The noise levels from the commercial Schmidt Boelter gauge was minimized due to the presence of adequate built-in filters for signal smoothing.

The maximum heat flux measured by using the commercial Schmidt Boelter gauge was 35 kW/m^2 at 295 seconds. The original sensor (Sullivan and McDonald) measured a maximum of 37 kW/m^2 at 325 seconds while the modified sensor measured 33 kW/m^2 at 310 seconds. The estimates of maximum heat fluxes for both the modified and original sensors were within 2 kW/m^2 of those measured by the Schmidt-Boelter gauge. However, the response time to the maximum heat flux of the modified sensor was within 4% of that of the commercial Schmidt-

Boelter gauge compared to 10% for the original sensor. This indicates that the modified sensor had a slightly improved response time to the applied heat load.

At the 0.152 m stand-off distance, there was less agreement between the measured incident heat fluxes among the custom sensors and the Schmidt-Boelter gauge. The increased stand-off distance resulted in lower heat flux measurements and slower response times for all the sensors as shown in Fig. 3-1(b). The maximum heat flux measured by the commercial Schmidt-Boelter gauge was 30 kW/m² at 360 seconds. The original sensor measured a maximum of 35 kW/m² at 400 seconds while the modified sensor measured a maximum of 31 kW/m² in 425 seconds. The measured maximum heat fluxes of the modified sensor were within 1 kW/m² of the Schmidt-Boelter gauge compared to 4 kW/m² for the original sensor. The response time to the maximum heat flux of the modified sensor was within 17% of the commercial Schmidt-Boelter gauge compared to 11% for the original sensor. The faster response time can be attributed to the higher thermal conductivity of the copper material (approximately 400 W/m-K at 300 K [59]) of the commercial Schmidt-Boelter gauge. The custom sensors were fabricated from aluminum metal with a thermal conductivity of approximately 240 W/m-K at 300 K [59].

To investigate the effects of natural convection in a mixed radiation convection environment, the dimensionless Rayleigh number (Ra) was examined at the 0.102 m and 0.152 m stand-off distances, where the problem was assumed to be flow over a vertical plate subjected to uniform surface heat flux. The Rayleigh number is:

$$\text{Ra}_H = \frac{g\beta(T_s - T_\infty)H^3 \text{Pr}}{\nu^2}, \quad (3-1)$$

where g is gravity, β is the compressibility factor of the fluid, $(T_s - T_\infty)$ is the temperature difference between the surface of the sensor and the ambient surroundings, H is the height of the sensor, Pr is the Prandtl number, and ν is the kinematic viscosity of the fluid. The Rayleigh number confirms the possibility of free convective currents at the front face of the sensor, further increasing the energy loss due to convection [60]. To obtain an estimate of the heat loss due to convection at the 0.102 m and 0.152 m stand-off distances, it was noted that the temperature difference between the surface of the sensor and the ambient surroundings was approximately 170 K and 120 K, respectively (based on the actual maximum measured temperatures during the tests). The properties of air were found at the film temperature [61] and are shown in Table 3-1. The Rayleigh number at the 0.102 m and 0.152 m was calculated to be 8.0×10^5 and 7.0×10^5 , which is below the critical Rayleigh number (10^9) for transition from laminar to turbulent free convective flow [60]. Also, the boundary layer approximation for free convection was valid since the Rayleigh number was greater than the critical Rayleigh number = 10^4 [60].

Table 3-1: Properties of air at film temperature [61].

Standoff Distance (m)	Film Temp. (K)	k (W/mK)	Pr	ν (m ² /s)	β (1/K)
0.102	378	0.03095	0.7090	2.400×10^{-5}	2.65×10^{-3}
0.152	370	0.03150	0.7111	2.306×10^{-5}	2.70×10^{-3}

The average convective heat transfer coefficient was calculated by using the similarity solution given by Jiji [60]. The average heat transfer coefficient, \bar{h} at the 0.102 m and 0.152 m stand-off distance was calculated to be 11.60 W/m²K and 11.30 W/m²K, respectively. With Newton's law of cooling [60],

$$q'' = \bar{h}(T_s - T_\infty). \quad (3-2)$$

The estimated heat flux lost due to free convection from the surface of the sensor was approximately 2.00 kW/m² at the 0.102 m stand-off distance and 1.43 kW/m² at the 0.152 m stand-off distance. This result indicates that there was heat loss due to free convection during the tests that were conducted at the varying stand-off distances. The estimates of the free convective losses that occur were insignificant compared to the measured heat fluxes that were greater than 30 kW/m². It should be noted that the temperature data that was used to calculate the heat lost due to convection were at the maximum heat flux for each test. As the temperature difference between the surface of the sensor and the ambient surroundings decreases, the heat flux lost due to free convection will also decrease.

The main factor that was pertinent for reduction in the heat flux at the increased stand-off distance was the reduction in radiant power. Based on Fig. 3-2, the view factor at the 0.152 m stand-off distance was determined to be approximately 50% of the maximum energy output from the radiant heater and that was incident on the sensors, compared to 60% at the 0.102 m stand-off distance.

3.2 MASS LOSS CALORIMETER TESTS

High Heat Flux Scenario. Previous research has shown that the heat flux of burning surface vegetative fuels ranges from 20 to 80 kW/m² [55]. For the purposes of this current study, high heat flux scenarios will be those in which the incident heat flux on the sensor is 40 kW/m² or higher. The resulting incident heat fluxes that were estimated from the heat flux sensors for one

of the representative tests conducted with the mass loss cone are shown in Fig. 3-3(a). The response of the sensor during the tests, where abrupt changes of heat flux were induced, can be seen in the figure. Once the shutter on the cone calorimeter was opened on each cycle, it was observed that steady-state was not achieved immediately. The Schmidt-Boelter gauge achieved steady state within 10 seconds after opening the shutter while the custom sensors achieved steady-state within approximately 20 seconds. The faster response time of the Schmidt-Boelter gauge can be attributed to the higher thermal conductivity of the copper material construction. At the end of the tests, beyond 120 s and 300 s, there were deviations in the measured heat flux between the custom sensors and the Schmidt-Boelter gauge. This deviation was due to the emitted radiation from the custom sensors to the shutter of the mass loss cone and ultimate reflection back to the sensors. This also occurred with the Schmidt-Boelter gauge since it measured a small heat flux at the end of the test. However, due to its smaller surface area, the measured heat flux was lower than that which was estimated by the custom sensors. This deviation was also observed by Sullivan and McDonald [20]. The influence of water cooling in the Schmidt-Boelter gauge was also a factor.

From the transient heat flux curve shown in Fig. 3-3(a), there is close agreement between the measured heat flux values of the Schmidt-Boelter gauge and those measured by the custom sensors once steady-state operation was achieved. The agreement became more pronounced on the second cycle, after 180 s, and after achieving steady-state. The targeted heat flux from the mass loss cone was 40 kW/m^2 . It was observed that, at steady-state, the heat flux values fluctuated slightly. This level of noise was due to the unsteady forced convection caused by an exhaust fan within the mass loss cone and the small clearance between the edge of the mass loss cone and the sensors. The average steady-state heat flux that was measured by using the

Schmidt-Boelter gauge was $37 \pm 1 \text{ kW/m}^2$ ($n = 240$), $34 \pm 3 \text{ kW/m}^2$ ($n = 240$) for the original sensor, and for the modified sensor, it was $35 \pm 2 \text{ kW/m}^2$ ($n = 240$). The modified sensor produced slightly less variations in the heat flux and the average steady-state incident heat flux was in closer agreement to that measured by the commercial Schmidt-Boelter gauge.

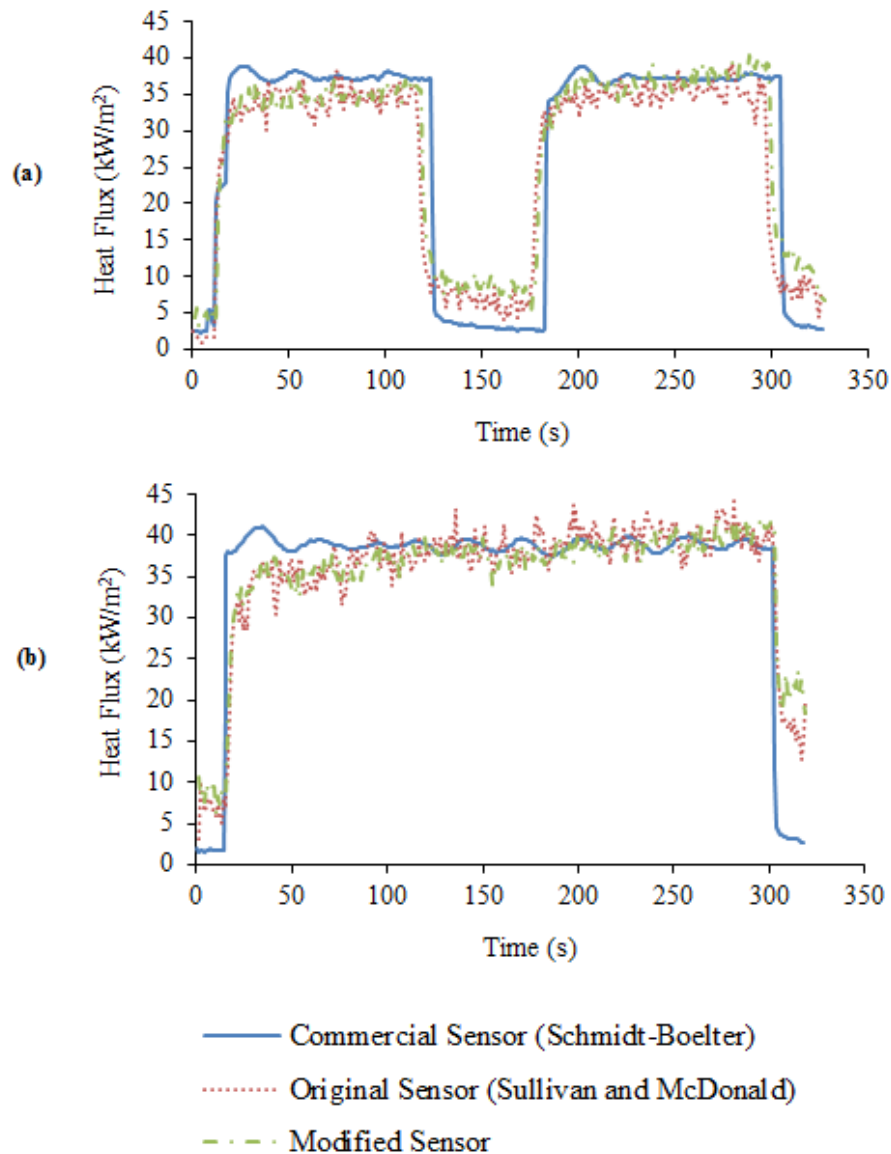


Figure 3-3: Incident heat flux curve from the mass loss cone tests at 40 kW/m^2 over (a) short, abrupt time periods and (b) an extended time period.

In industrial practice, the measurement and estimation of incident heat fluxes from high heat load sources such as wildland fires will need to be captured over long time periods [52]. Figure 3-3(b) shows transient heat flux results from the original sensor, the modified sensor, and the Schmidt-Boelter gauge for extended operation of the mass loss cone. The average steady-state heat flux that was measured using the Schmidt-Boelter gauge was $39 \pm 1 \text{ kW/m}^2$ ($n = 300$), for the original sensor, it was $38 \pm 3 \text{ kW/m}^2$ ($n = 300$), while for the modified sensor it was $38 \pm 2 \text{ kW/m}^2$ ($n = 300$). The custom sensors (original and modified) were able to measure intense heat fluxes over extended time periods similar to those observed in field experiments [55]. This suggests that the modified sensor would also perform satisfactorily under conditions of outdoor field fires. At steady-state, the temperatures at any given point in the custom-made sensors are constant, even though there is a spatially varying temperature distribution. The absence of transient temperature variation in the sensors eliminates errors due to response of the sensors, and improves agreement among the predicted incident heat fluxes.

Low Heat Flux Scenario. In order to observe the response of the sensors exposed to low incident heat fluxes, the mass loss cone test was conducted at a targeted heat flux of 15 kW/m^2 . The resulting transient heat fluxes for one of the representative tests over an extended time period, is shown in Fig. 3-4.

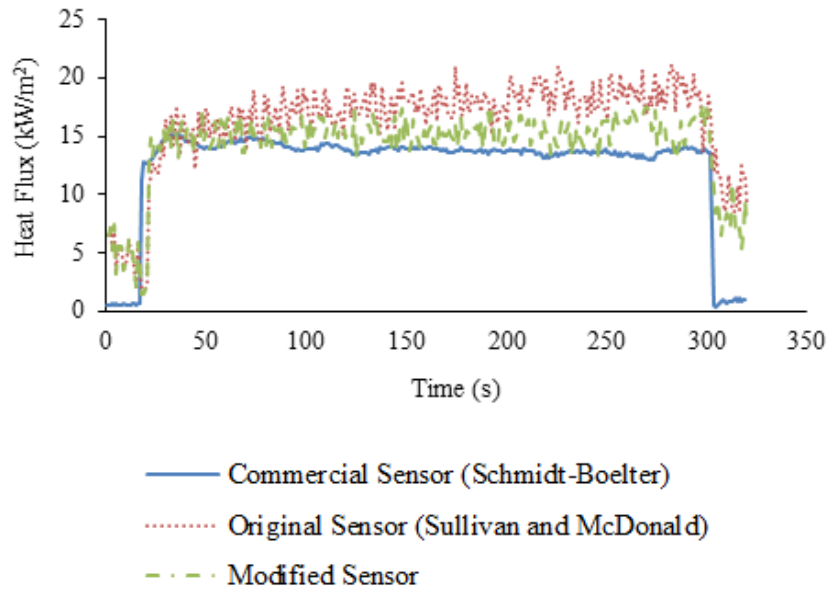


Figure 3-4: Incident heat flux curve from the mass loss cone tests at 15 kW/m^2 over an extended period.

The noise in the data from the sensors, as shown in Fig. 3-4, became more pronounced at lower steady-state incident heat fluxes as a result of the relative increased impact of forced convection at the surface of the sensors with the absence of adequate filters. For the custom sensors, the smaller temperature difference resulted in a larger error. The average steady state heat flux that was measured using the Schmidt-Boelter gauge was $14 \pm 0.5 \text{ kW/m}^2$ ($n = 300$), for the original sensor, it was $17 \pm 4 \text{ kW/m}^2$ ($n = 300$), while for the modified sensor, it was $15 \pm 2 \text{ kW/m}^2$ ($n = 300$). These tests showed closer agreement between the measured incident heat flux values of the commercial Schmidt-Boelter gauge and those estimated by using the modified sensor. The modified sensor also had less variation in the steady-state incident heat flux compared to the sensor developed by Sullivan and McDonald [20], as evidenced by the lower standard deviation reported with the average steady-state heat flux.

3.3 CONTROLLED CROWN FIRE TEST

The modified heat flux sensor performed well in the electric-powered radiant panel and mass loss cone tests that were conducted. It was then necessary to evaluate the performance of the custom-built sensors in a real fire scenario, such as a high intensity crown fire. The surface fuels in a plot were ignited and quickly became a fast moving crown fire with observed laddering from the surface to aerial fuels. The transient heat flux calculated from the model as measured by the original and modified sensors is shown in Fig. 3-5.

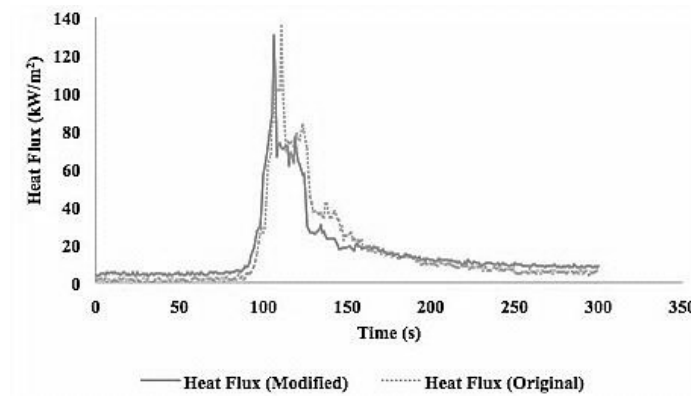


Figure 3-5: Transient incident heat flux curve from the controlled crown fire.

The heat flux does not begin at zero due to starting the logger long before the fire was ignited. The initial energy originated from the solar radiation incident on the surface of the sensors after being left in position for over two hours. The heat flux increased rapidly as the crown fire propagated and the flame engulfed the sensors completely and continued to burn past it, as shown in Fig. 3-6.

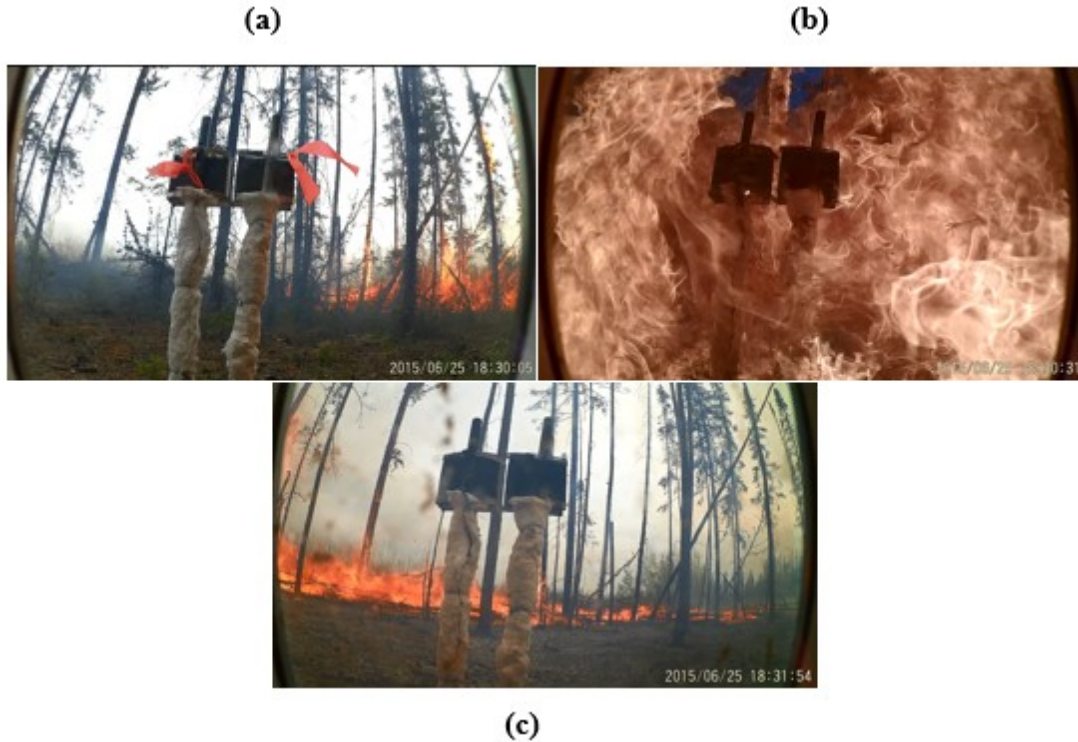


Figure 3-6: Images of the heat flux sensors under extreme crown fire conditions (a) flame front approaches, (b) sensors fully engulfed in flames, (c) after the flame passes the sensors.

The delay observed in Fig. 3-5 is as a result of the sensor placement relative to the path of the fire. The original heat flux sensor observed a maximum heat flux of approximately 136 kW/m^2 while the modified sensor observed a maximum of approximately 132 kW/m^2 . The maximum heat fluxes measured are similar in magnitude to those observed by Frankman et al. [14]. The difference in the measured maximum heat flux between the sensors was estimated to be approximately 3%. After the fire had passed, a small amount of energy remained due to some small spot fires that were still burning. The crown fire test provided evidence of the successful performance of the heat flux sensors under high heat load, direct flame conditions.

3.4 UNCERTAINTY ERROR ANALYSIS

The propagation of uncertainty errors in the heat flux estimates was determined by using Eq. (3-3), which is based on a similar analysis conducted by Sullivan [52]. Equation (3-3) states

$$\left(\frac{\omega_{q_{net}}}{q_{net}}\right)^2 = \left(\frac{\omega_{\Delta T}}{\Delta T}\right)^2 + \left(\frac{[(\omega_L)^2 + (\omega_d)^2]^{1/2}}{(L-d)}\right)^2 + 8\left(\frac{\omega_{T_1(t)}}{T_1(t)}\right)^2 + 8\left(\frac{\omega_{T(d,t)}}{T(d,t)}\right)^2 \quad (3-3)$$

In Eq. (3-3), ω is the error variable of the measured quantity, L is the thickness of the sensor, d is the depth into the sensor where a thermocouple is located, $T_1(t)$ is the backside temperature, $T(d,t)$ is the temperature at location d in the sensor, and ΔT is the measured differential temperature. The data from the mass loss cone tests (see Table 3-2) were used in Eqs. (2-2) and (3-3) to estimate the errors in the estimates of the incident heat fluxes obtained from the original sensor and the modified sensor, respectively.

Table 3-2: Data values from the mass loss cone test for calculation of error values.

Test	High Heat Flux (Approximately 42 kW/m ²)		Low Heat Flux (Approximately 13 kW/m ²)	
	Original Heat Flux Sensor	Modified (J-Type) Heat Flux Sensor	Original Heat Flux Sensor	Modified (J-Type) Heat Flux Sensor
<i>t</i> (s)	234	271	26	20
<i>T</i>(<i>d, t</i>) (°C)	271.74	259.60	107.83	107.31
<i>T</i>₁(<i>t</i>) (°C)	268.73	256.14	106.79	106.10
<i>L</i> (mm)	22.23	22.23	22.23	22.23
<i>d</i> (mm)	3.18	3.18	3.18	3.18
<i>T</i>_∞ (°C)	22	22	22	22
Heat Flux (kW/m²)	42.31	42.26	13.00	13.14
Calculated Error:	54%	32%	110%	90%

The error values obtained using the original sensor design by Sullivan and McDonald for the low heat flux condition was 110% and for the high heat flux condition, it was 54%. On implementing the new thermocouple circuitry, and by using the differential temperature, rather than the absolute temperatures, the error in the low heat flux condition was reduced to 90% while that in the high heat flux condition was reduced to 32%. As stated in Section 2.1, the actual thermocouple errors may in fact be less than the manufacturer's stated limit of error of 1.1°C, resulting in lower and more acceptable errors in the heat flux estimates. To determine the actual errors in the heat flux estimates, would require the actual thermocouple errors to be determined through rigorous calibration procedures.

To reduce the errors further, the J-Type thermocouples could be replaced by R- or S-Type thermocouples. The R- or S-Type thermocouples have a manufacturer-rated error of 0.6°C and using the aforementioned data in this study, they would possibly yield an error of 50% in the low heat flux condition and 19% in the high heat flux condition, which is a significant reduction in the errors obtained when the J-Type thermocouples are used. This option would however prove to be more expensive.

3.5 WILDLAND FIRE CHEMICAL EVALUATION

3.5.1 Radiant Heater Evaluation

An evaluation of the performance of the radiant panel heater was necessary to determine the heat fluxes and temperatures to which the vegetative fuel samples at the specified stand-off distance 0.102 m (4 in). The result from the evaluation that was conducted at the standoff distance is

shown in Fig. 3-7. The figure shows that as the radiant heater panel surface temperature increases, there is a resulting proportional increase in the heat flux at the stand-off distance.

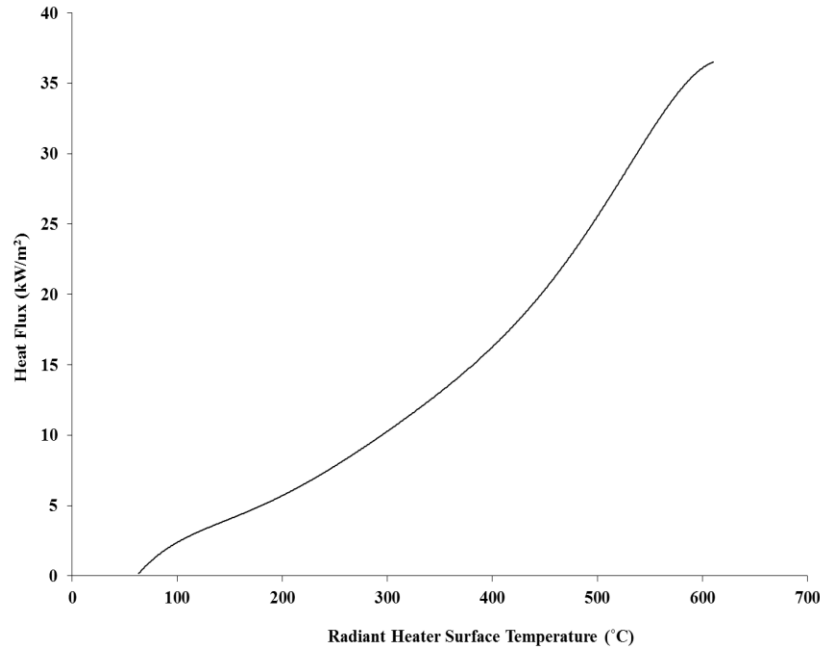


Figure 3-7: Relationship between the heat flux at the stand-off distance of 0.102 m and the radiant heater surface temperature.

Based on the results from the evaluation, placing the vegetative fuel samples at the specified stand-off distance from the heater was adequate to provide the required heat flux of 18 kW/m² for ignition during the heating up process. This required heat flux for ignition of the vegetative was identified by Sullivan [52] during a similar study on vegetative fuels. The view factor from the electric-powered radiant heater was similar to that determined during the radiant heater test in Section 3.1 at the 0.102 m stand-off distance. Therefore, the maximum available heat flux at the specified stand-off distance at the vegetative fuel sample was approximately 54 kW/m².

3.5.2 Heat Flux Data

The main feature of the test methodology was the incorporation of a heat flux sensor to determine the ignition time of vegetative fuel samples. The data gathered from the heat flux sensors was therefore investigated. Figure 3-8 shows a curve of the incident heat flux on the original sensor that originated from the heated, untreated vegetative fuel. The curve shows that after approximately 190 seconds of heating, the heat flux originating from the fuel increases suddenly, which is indicative of ignition that caused flaming. Given the level of noise in the data, the glowing ignition time cannot be confidently identified using this method. As the sample burned, the heat flux increased to a maximum value, and decreased as the material was consumed by the fire. Similar interpretations of signals have been presented, where a relation between the patterns of voltage signals indicated the occurrence of a physical phenomenon or a change in a measured parameter [62].

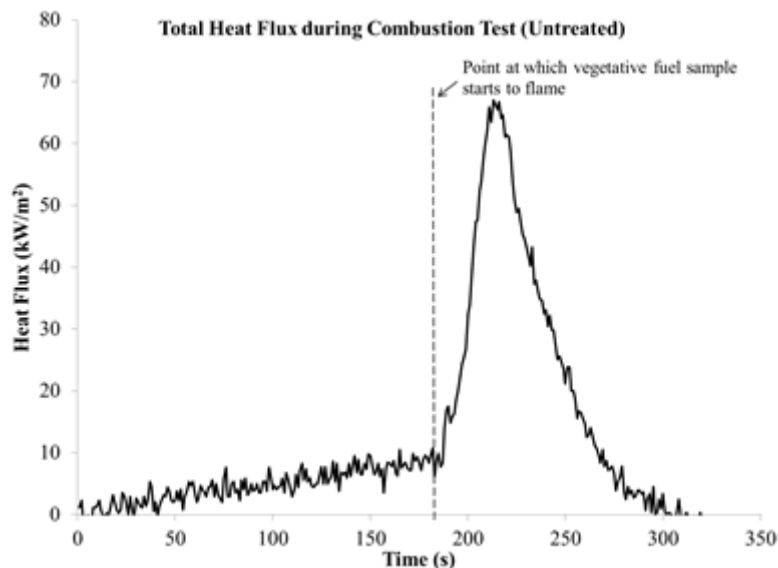


Figure 3-8: Mean ignition time of an untreated vegetative fuel sample from transient heat flux data (original heat flux sensor by Sullivan and McDonald).

The modified heat flux sensor was also used to evaluate the transient heat flux that was generated during the heating of the fuel. Figure 3-9 shows a curve of the incident heat flux on the modified sensor that originated from the heated, untreated vegetative fuel. The curve is similar to that of the original sensor where, after approximately 190 seconds of heating, the heat flux originating from the fuel increases suddenly, which is indicative of ignition that caused flaming. This further validates the accuracy of the modified sensor following the mass loss cone tests. The difference observed between Figs. 3-8 – 3-9 for the maximum heat flux incident on the sensors at ignition can be attributed to the non-uniformity and inhomogeneity of the composition of the vegetative fuel samples that were used.

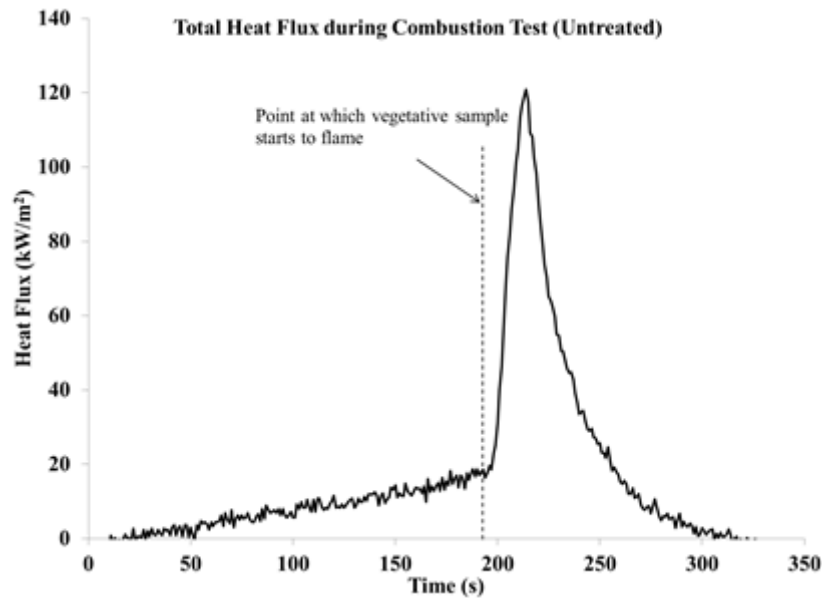


Figure 3-9: Mean ignition time of an untreated vegetative fuel sample from transient heat flux data (modified heat flux sensor).

3.5.3 Transient Mass Loss Data

Transient mass loss data was used to validate the time-to-ignition that initiated flaming of the fuel as measured from the heat flux sensors. A graph of the transient mass of an untreated vegetative fuel sample is shown in Fig. 3-10. The time at which flaming was initiated (190 seconds) is indicated by a sharp, nearly singular, decrease in the mass of the fuel as it is consumed during the burning process. Given the level of noise in the data, the glowing ignition time cannot be confidently identified using this method.

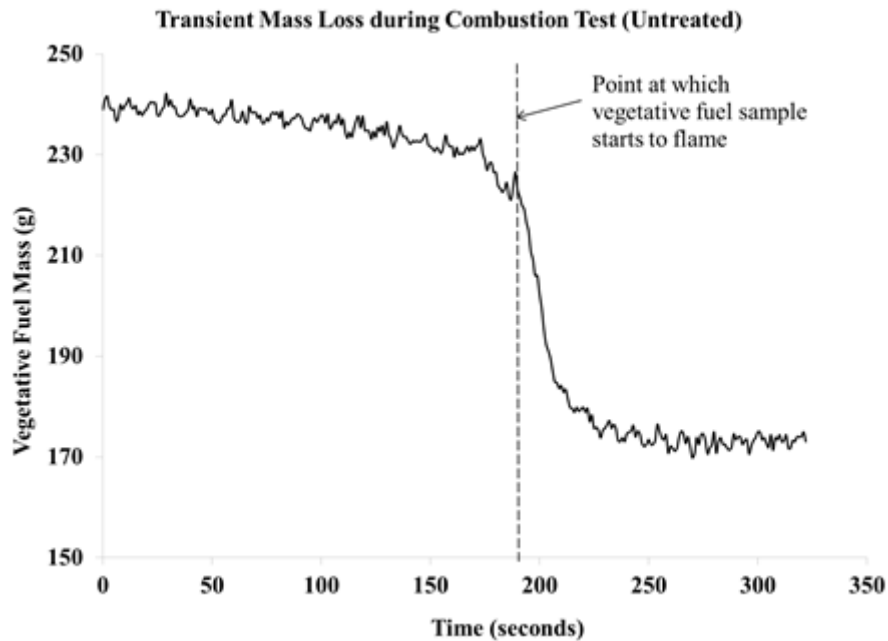


Figure 3-10: Mean ignition time of an untreated vegetative fuel sample from transient mass data.

Comparison of the mean ignition times obtained from the heat flux (both the original and modified sensors) and transient mass loss data are presented in Table 3-3. The results show that the variation in the ignition times required for flaming of the fuel, as determined from data from the two methods, was less than 2%. The results from the two methods were also in accord with

respect to the time at which the flame was extinguished and the burnt fuel began to cool. From Figs. 3-8 – 3-10 for the untreated vegetative fuel sample, that time appears to be approximately 225 seconds after initial heating of the fuel. For the transient mass, the mass did not decrease further beyond 225 seconds and for the transient heat flux, the heat flux began to decrease from a maximum at approximately the same time. Table 3-3 also presents ignition time data for the treated vegetative fuels. The transient heat flux and mass loss curves for the treated fuel samples were characteristically similar to those of the untreated fuel, with quantifiable differences in the ignition time due to the treatment type.

Table 3-3: Comparison of average flaming ignition time from the heat flux and mass loss data.

Treatment	Flaming Ignition Time (sec) – Original Sensor Heat Flux	Flaming Ignition Time (sec) – Modified Sensor Heat Flux	Flaming Ignition Time (sec) – Mass Loss
Untreated	182	180	184
Water	210	208	209
Gel	308	304	307
Foam	341	338	342
Long-Term Retardant	<i>No Ignition (> 900 seconds)</i>		

3.5.4 Wildfire Chemicals Performance

The mean ignition times, based on glowing ignition and flaming ignition, for each of the treatments that were explored are shown in Table 3-4, along with the standard deviation and number of tests (*n*) that were conducted. The glowing ignition time data that are presented in the table were gathered manually with the use of a stopwatch and visual observation. The data for

the time to flaming ignition were determined from the transient heat flux (using the modified sensor developed in this present study) and mass loss measurements. Glowing ignition is characterized by solid phase combustion of the charred products, which is then immediately followed by flaming ignition (combustion of volatile gases). The heat flux and transient mass loss data were not able to indicate the time at which glowing ignition occurred.

Table 3-4: Results from the burn tests for the different wildfire chemicals.

Treatment	Glowing Ignition Time (sec.) - Visually	Flaming Ignition Time (sec.) – Modified sensor	Flaming Ignition Time (sec.) – Visually
Untreated	167 ± 3 (<i>n</i> = 12)	180 ± 4 (<i>n</i> = 12)	184 ± 8 (<i>n</i> = 12)
Water	179 ± 10 (<i>n</i> = 15)	208 ± 8 (<i>n</i> = 15)	215 ± 13 (<i>n</i> = 15)
Gel	270 ± 25 (<i>n</i> = 12)	304 ± 22 (<i>n</i> = 12)	308 ± 25 (<i>n</i> = 12)
Foam	309 ± 28 (<i>n</i> = 10)	338 ± 38 (<i>n</i> = 10)	339 ± 40 (<i>n</i> = 10)
Long-Term Retardant	<i>No Ignition (> 900 seconds)</i>		

The results presented in Table 3-4 show the variations in the ignition time (both glowing and flaming ignition) for the different treatments, with the untreated fuel serving as an experimental control. The results confirm that the flaming ignition time as determined from the modified sensor is in close agreement with the flaming ignition time obtained visually. There was a delay in the transition of the ignition time from glowing ignition to flaming ignition as shown in the table. As the vegetative fuel is heated by the radiant heater, off-gassing and charring is initiated, followed by the combustion of volatile gases.

From the results, the most effective treatment that delayed ignition was the long-term retardant-based chemical. As expected, the untreated sample had the shortest ignition time. The long-term

fire retardant gains its effectiveness through the use of chemicals, which alters the combustion process. The active ingredient, salt, permits pyrolysis at a lower temperature and promotes the formation of water (H₂O), carbon dioxide (CO₂) gas, and char, at the expense of flammable gases. The vegetative sample itself does not burn. Rather, the gases that are produced through pyrolysis ignite when the “flash point” is reached, and provide the heat necessary to produce more flammable gases. This “flash point” was not attainable using this test methodology. However, incorporation of a reliable piloted ignition source may influence the ignition of the long-term retardant-treated samples.

3.5.5 Statistical Analysis

A statistical analysis, using a two sided *t*-test at a significance level of $\alpha = 0.05$, was conducted on the mean time to flaming ignition (as measured by the developed modified sensor) to determine whether the results from the burn test were statistically different for the various treatments. A review of the *t*-test hypothesis procedure has been provided elsewhere [63]. The hypothesis is stated as follows, that

$$H_0 : \mu_1 = \mu_2 \quad \text{Null Hypothesis} \quad (3-4)$$

$$H_1 : \mu_1 \neq \mu_2 \quad \text{Alternative Hypothesis} \quad (3-5)$$

where μ_1 = mean ignition time of treatment type A and μ_2 = mean ignition time of treatment type B.

The appropriate test statistic to use for comparing the average ignition time is:

$$t_o = \frac{\bar{y}_1 - \bar{y}_2}{S_p \sqrt{\frac{1}{n_1} + \frac{1}{n_2}}} \quad (3-6)$$

where \bar{y}_1 and \bar{y}_2 = mean ignition time of treatment A and B, respectively, n_1 and n_2 = sample sizes of A and B, respectively, and S_p = estimate of the common variance.

In order to determine if $H_0: \mu_1 = \mu_2$ should be rejected, t_o is compared with the t -distribution tables with $n_1 + n_2 - 2$ degrees of freedom. If $|t_o| > t_{\alpha/2, n_1+n_2-2}$, where $t_{\alpha/2, n_1+n_2-2}$ is the upper $\alpha/2$ percentage point of the t -distribution with $n_1 + n_2 - 2$ degrees of freedom, H_0 should be rejected and this would indicate that the means differ [63]. The results from the t -tests are shown in Table 3-5 for the different wildland fire chemical treatments.

Table 3-5: t -test results of the average (mean) flaming ignition times through comparison of the wildfire chemicals.

Treatment	Mean Ignition Time (s)	t -Value Calculated	t -Value Distribution Tables ⁶³
Untreated vs. Water	180 ± 4 ($n = 12$) 208 ± 8 ($n = 15$)	11.0	1.7
Untreated vs. Foam	180 ± 4 ($n = 12$) 338 ± 38 ($n = 10$)	14.4	1.7
Untreated vs. Gel	180 ± 4 ($n = 12$) 304 ± 22 ($n = 12$)	19.2	1.7
Water vs. Foam	208 ± 8 ($n = 15$) 338 ± 38 ($n = 10$)	12.9	1.7
Water vs. Gel	208 ± 8 ($n = 15$) 304 ± 22 ($n = 12$)	15.7	1.7
Foam vs. Gel	338 ± 38 ($n = 10$) 304 ± 22 ($n = 12$)	2.6	1.7

Based on the results presented in Table 3.5, and since the calculated t -values in each case is greater than the t -value from the distribution tables, it can be concluded that the mean flaming ignition times are statistically different for the different treatments. This result suggests that the test methodology developed is effective in comparing the different wildfire chemicals.

4. THERMAL CANISTER DEVELOPMENT

The methodology for evaluating the performance of wildfire chemicals required measurement of the time-to-ignition based on heat flux data. However, the incident heat flux data by itself may not be considered a quantity that allows for a complete evaluation of the relative performance of wildfire chemicals. From the combustion process, the incident heat flux may vary based on the orientation and position of the heat flux sensor relative to the burning sample. Based on the design of the custom-built thermocouple-based heat flux sensors, it may be possible to develop a suitable method to measure the total heat release rate from the combustion process which takes advantage of the heat flux data. From the literature review, it was found that the heat release rate was considered to be a significant property for the purpose of product evaluation and performance, and the heat release rate is typically measured by using a calorimeter [50-51]. The idea of a custom-built thermal calorimeter, hereinafter known as the “Thermal Canister,” was conceptualized in this present study. The calorimeter that was developed would be an expansion on the concept of the custom-built thermocouple-based heat flux sensors. The thermal canister was designed to measure the heat release rate along with the ignition time from a burning fuel, in a fashion similar to that of the sensible enthalpy calorimeter [50]. Details of the mathematical modelling and fabrication of the thermal canister are discussed further in the following sections.

4.1 THERMAL CANISTER FABRICATION AND OPERATION

The thermal canister was fabricated completely from 6061 aluminum plate. The dimensions for each of the canister walls were 0.508 m x 0.279 m x 0.01905 m (See Appendix A). The total

internal volume of the thermal canister was approximately 0.033 cubic meters. The canister walls, cover plate, and exhaust pipe were fabricated for easy assembly/or disassembly for the mounting/or dismounting of the samples. The parts of the canister were connected by socket head cap screws. The connection points were sealed using M-board insulation (M-board, Industrial Insulation Group, Augusta, GA, USA) to prevent the escape of exhaust product from the system. The internal faces of the canister walls were painted with a high temperature black spray paint similar to the custom-built heat flux sensors to increase the emissivity so that it approached that of an ideal black body and also to enhance absorption of almost all radiation heat transfer. In each wall and cover, eight 1.98 mm (0.078 in.) diameter holes were drilled to allow for insertion of the thermocouples, as shown in Fig 4-1. The thermocouples that were located at the center of the walls and cover were used to validate the model experimentally. The data from the thermocouples was used to generate transient temperature profiles and to establish the boundary conditions at the internal and external face of each wall. Similar to the custom-built heat flux sensors, Type J, 30 gauge thermocouples were selected. The thermocouples were wired to measure the differential temperature as shown in Fig. 2-2. A 6.35 mm diameter hole was drilled into the exhaust pipe to accommodate the insertion of a Pitot tube and thermocouple.

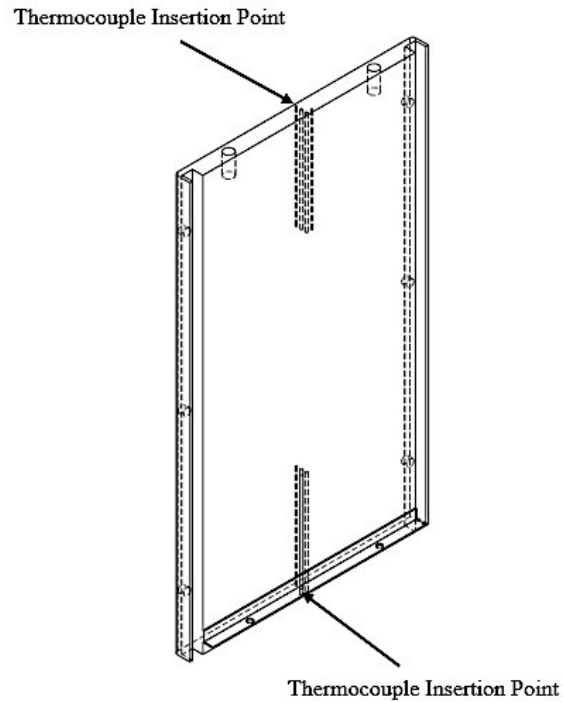


Figure 4-1: Representation of the thermal canister walls.

The thermal canister's complete configuration included a 0.31 m x 0.31 m (12 in x 12 in) electric-powered radiant heater (Omegalux QH-121260, Omega Engineering, Inc., Laval, QC, Canada). The radiant heater was rated at 240 VAC, 1 phase, 1660 – 8640 watts, which allowed for incident heat fluxes of up to 90 kW/m^2 , with a maximum surface temperature rating of the heater of up to 980°C . The radiant heater was used to provide a uniform heat flux to ignite the test samples. The heater was arranged horizontally below the thermal canister at a distance of 0.102 m. The final system configuration is shown in Fig. 4-2.

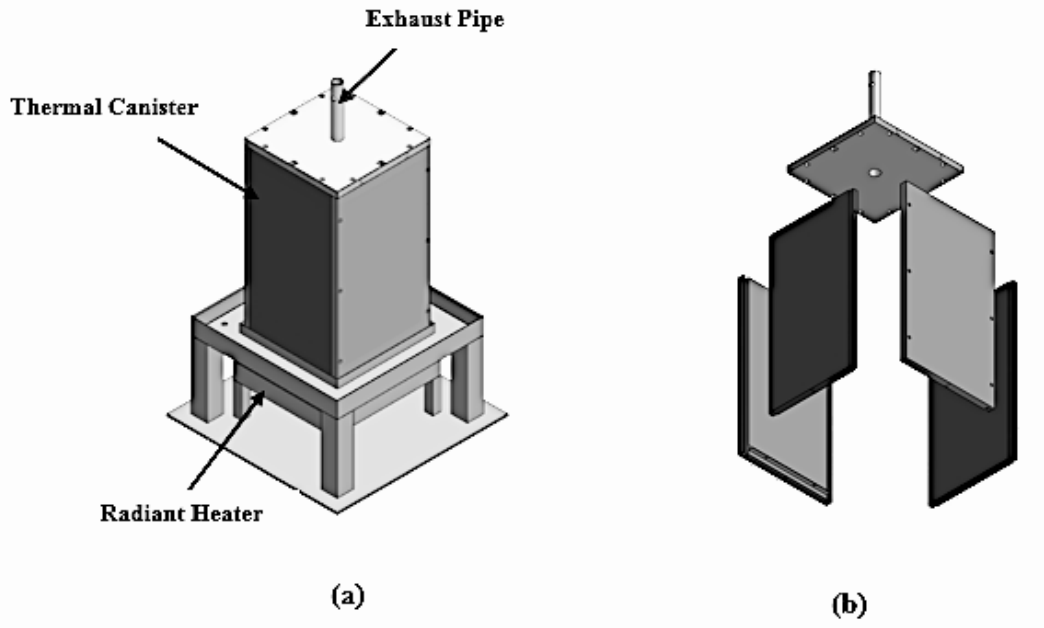


Figure 4-2: a) Thermal canister configuration, b) exploded view of the thermal canister.

4.2 THERMAL CANISTER MATHEMATICAL MODEL

A heat conduction model was developed to determine the temperature distribution in the thermal canister, containing the fuel samples to be combusted, was based on the assumption of uniform heating of a rectangular-shaped body. Similar to the heat flux sensor developed by Sullivan and McDonald [20], the model was idealized as a one-dimensional, finite-length scale problem. It was assumed that heat transfer across the exposed walls of the canister was relatively uniform. In addition, the high thermal diffusivity of aluminum facilitated the reduction of any thermal fluctuations that may occur.

The separation of variables method was used to solve for the temperature distribution in each plate and then determine the total incident heat flux on all the plates. In order to model the

thermal canister, the walls were subdivided into two even different sections along lines of symmetry as shown in Fig. 4-3a. Consider the following plate with thickness, W as shown in Fig. 4-3b:

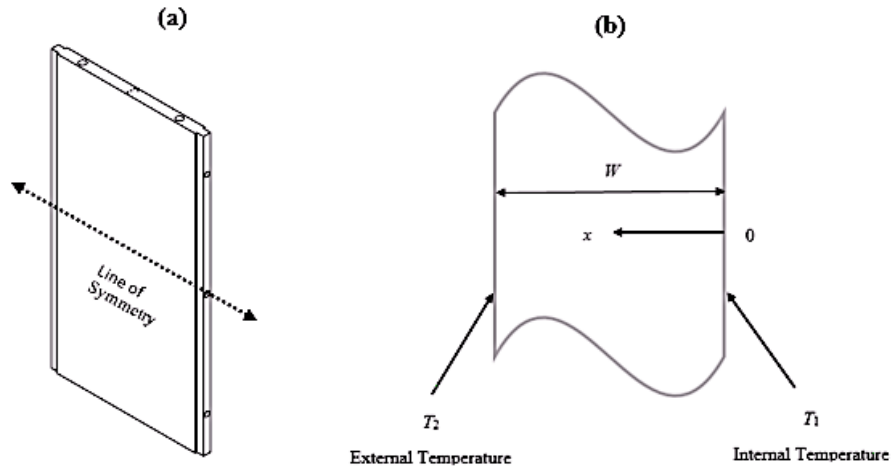


Figure 4-3: (a) Representation of the thermal canister wall showing line of symmetry and (b) schematic for the mathematical model.

To determine whether the wall can be assumed to be one-dimensional, the Biot number (Bi) was verified. If the Biot number is less than 0.1, then the problem can be modelled as one-dimensional [64]. The Biot number is defined as:

$$Bi = \frac{h\delta}{k}, \quad (4-1)$$

where h is the heat transfer coefficient, k is the thermal conductivity of the wall material, and δ is the half thickness. Aluminum 6061 was the material chosen based on its high thermal diffusivity, high thermal conductivity, high melting point of approximately 580 to 650°C [65], and relatively constant thermal conductivity at elevated temperatures beyond 0°C [66]. The heat transfer coefficient, h , was estimated to be 13.3 W/m²K, and was based on the assumption of free

convective flow over a vertical plate subjected to uniform heat flux as determined by Sullivan and McDonald for the maximum temperature differences expected in wildland fire conditions [20]. The thermal conductivity of the material, k , was 167 W/mK [59] and the half thickness, δ was calculated to be 0.0095 m. Therefore, the Biot number is:

$$\text{Bi} = \frac{13.3 \text{ W/m}^2\text{K} \times 0.0095 \text{ m}}{167 \text{ W/m}^2\text{K}} = 0.00076 .$$

Since $\text{Bi} = 0.00076 \lll 0.1$, the one dimensional model assumption is justified.

The one-dimensional governing equation for the temperature distribution in the canister plate shown in Fig. 4-3 is given by

$$\frac{\partial^2 T}{\partial x^2} = \frac{1}{\alpha} \frac{\partial T}{\partial t} , \tag{4-2}$$

where α is the thermal diffusivity of the material, which is defined as $\alpha = k/\rho c_p$, and represents the ability of a material to adjust to temperature changes.

The boundary and initial conditions are given by:

$$T(0,t) = T_1(t) , \tag{4-3}$$

$$T(W,t) = T_2(t) , \tag{4-4}$$

$$T(x,0) = T_i . \tag{4-5}$$

Since the boundary conditions of Eqs. (4-3) and (4-4) are non-homogeneous, the method of superposition and separation of variables was used to solve the governing equation. Therefore, a solution of the form

$$T(x,t) = \Psi(x,t) + \Phi(x). \quad (4-6)$$

was assumed, where Ψ depends on x and t for the homogenous solution and Φ depends on x , only for the particular solution.

Equation (4-6) was substituted into the governing equation of Eq. (4-2) to yield

$$\frac{\partial^2 \Psi}{\partial x^2} + \frac{\partial^2 \Phi}{\partial x^2} = \frac{1}{\alpha} \frac{\partial \Psi}{\partial t}. \quad (4-7)$$

The homogenous and non-homogeneous terms of Eq. (4-7) were separated into two equations, one for $\Psi(x,t)$ and the other for $\Phi(x)$ to give

$$\frac{\partial^2 \Psi}{\partial x^2} = \frac{1}{\alpha} \frac{\partial \Psi}{\partial t}, \quad (4-8)$$

$$\frac{\partial^2 \Phi}{\partial x^2} = 0. \quad (4-9)$$

Boundary conditions to solve $\Psi(x,t)$ and $\Phi(x)$ were obtained by substituting Eq. (4-7) into the boundary and initial conditions. Therefore, the boundary condition at $x = 0$ in Eq. (4-3) gives

$$\Psi(0,t) + \Phi(0) = T_1(t). \quad (4-10)$$

For a simple homogeneous problem, let

$$\Psi(0,t) = 0. \quad (4-11)$$

Therefore

$$\Phi(0) = T_1(t). \quad (4-12)$$

Similarly, substituting the boundary condition at $x = W$ in Eq. (4-4) gives

$$\Psi(W, t) + \Phi(W) = T_2(t). \quad (4-13)$$

Let

$$\Psi(W, t) = 0. \quad (4-14)$$

Therefore

$$\Phi(W) = T_2(t). \quad (4-15)$$

The initial condition gives

$$\Psi(x, 0) + \Phi(x) = T_i. \quad (4-16)$$

Rearranging Eq. (4-16) yields

$$\Psi(x, 0) = T_i - \Phi(x). \quad (4-17)$$

Starting with the simple linear ordinary differential equation, Eq. (4-9) was solved by integrating, yielding

$$\Phi(x) = Ax + B, \quad (4-18)$$

where A and B are the constants of integration. Application of the boundary conditions of Eqs. (4-12) and (4-15) to Eq. (4-18) gives the two constants of integration as

$$B = T_1,$$

$$A = \frac{1}{W}(T_2 - T_1).$$

Therefore, the solution becomes

$$\Phi(x) = \frac{1}{w}(T_2 - T_1)x + T_1. \quad (4-19)$$

The solution of $\Psi(x,t)$ in Eq. (4-8) is obtained using the method of separation of variables.

Therefore, a product solution was assumed in the form

$$\Psi(x,t) = X(x)\tau(t), \quad (4-20)$$

where X depends on x , only and τ depends on t , only.

Equation (4-8) was substituted into Eq. (4-20) to give

$$\frac{d^2 X}{dx^2} \tau = \frac{1}{\alpha} \frac{d\tau}{dt} X. \quad (4-21)$$

Separating the variables and setting the resulting equation equal to a constant, $\pm \lambda_n^2$, gives

$$\frac{d^2 X_n}{dx^2} \mp \lambda_n^2 X_n = 0, \quad (4-22)$$

$$\frac{d\tau_n}{dt} \mp \alpha \lambda_n^2 \tau_n = 0. \quad (4-23)$$

Since the x -variable has two homogeneous boundary conditions, the eigenvalue is positive.

Therefore, Eqs. (4-22) and (4-23) become

$$\frac{d^2 X_n}{dx^2} + \lambda_n^2 X_n = 0, \quad (4-24)$$

$$\frac{d\tau_n}{dt} + \alpha \lambda_n^2 \tau_n = 0. \quad (4-25)$$

For the case $n = 0$ ($\lambda_n = 0$), the equations become

$$\frac{d^2 X_0}{dx^2} = 0, \quad (4-26)$$

$$\frac{d\tau_0}{dt} = 0. \quad (4-27)$$

The simple ordinary differential equations of Eqs. (4-26) and (4-27) were solved by direct integration, which yields

$$X_0(x) = A_0 x + B_0, \quad (4-28)$$

$$\tau_0(t) = C_0. \quad (4-29)$$

where A_0 , B_0 , and C_0 are the constants of integration. Applying the boundary conditions of Eq. (4-11) and (4-14) and the initial condition (4-17) to Eqs. (4-26) and (4-27) gives a trivial solution

$$X_0(x) = 0,$$

$$\tau_0(t) = 0.$$

When n is greater than zero, integration of Eqs. (4-24) and (4-25) yields

$$X_n(x) = A_n \sin \lambda_n x + B_n \cos \lambda_n x, \quad (4-30)$$

$$\tau_n(t) = C_n e^{-\alpha \lambda_n^2 t}, \quad (4-31)$$

where A_n , B_n , and C_n are the constants of integration. Then applying the boundary condition from Eq. (4-11) yields

$$B_n(x) = 0.$$

Also, applying the boundary condition from Eq. (4-14) gives

$$A_n \sin \lambda_n W = 0.$$

Therefore, the characteristic equation for λ_n is

$$\lambda_n = \frac{n\pi}{W}, \quad \text{where } n = 1, 2, 3, \dots \quad (4-32)$$

Therefore, the complete homogeneous solution becomes

$$\Psi(x, t) = \sum_{n=1}^{\infty} a_n e^{-\alpha \lambda_n^2 t} \sin \lambda_n x, \quad (4-33)$$

where $a_n = A_n C_n$.

Applying the initial condition of Eq. (4-17) gives

$$T_i - \Phi(x) = \sum_{n=1}^{\infty} a_n \sin \lambda_n x. \quad (4-34)$$

To solve for a_n , the concept of orthogonality was applied [64]. The characteristic function, $\sin \lambda_n x$ in Eq. (4-34) are solutions to Eq. (4-24). Equation (4-24) was compared with the Sturm Liouville equation shown in Eq. (4-35) [64]:

$$\frac{d}{dx} \left[p(x) \frac{dT_n}{dx} \right] + [q(x) + \lambda_n^2 w(x)] T_n = 0, \quad (4-35)$$

where $p(x) = e^{\int a_1 dx}$, $q(x) = a_2 dx$, $w(x) = a_3 p(x)$.

For this problem, $a_1 = a_2$, $a_3 = 1$, $p(x) = w(x) = 1$, and $q(x) = 0$. Multiplying both sides of Eq. (4-34) by $\sin \lambda_n x$, integrating from $x = 0$ to $x = W$, and invoking orthogonality gives

$$\int_0^W [T_i - \Phi(x)] \sin \lambda_n x dx = a_n \int_0^W \sin^2 \lambda_n x dx ,$$

$$a_n = \frac{\int_0^W [T_i - \Phi(x)] \sin \lambda_n x dx}{\int_0^W \sin^2 \lambda_n x dx} ,$$

$$a_n = \frac{\int_0^W [T_i - \frac{1}{W}(T_2 - T_1)x + T_1] \sin \lambda_n x dx}{\int_0^W \sin^2 \lambda_n x dx} ,$$

$$a_n = \frac{\frac{-\lambda_n W(T_i + 2T_1 - T_2) \cos \lambda_n W + \lambda_n W(T_i + T_1) + (T_1 - T_2) \sin \lambda_n W}{\lambda_n^2 W}}{\frac{2\lambda_n W + \sin(2\lambda_n W)}{4\lambda_n}} ,$$

$$a_n = \frac{-4(\lambda_n W(T_i + 2T_1 - T_2) \cos \lambda_n W + \lambda_n W(T_i + T_1) + (T_1 - T_2) \sin \lambda_n W)}{\lambda_n W(2\lambda_n W + \sin(2\lambda_n W))} . \quad (4-36)$$

Substituting a_n into Eq. (4-33), the temperature distribution in the section becomes

$$T(x, t) = \frac{1}{W}(T_2 - T_1)x + T_1 + \sum_{n=1}^{\infty} a_n e^{-\alpha \lambda_n^2 t} \sin \lambda_n x . \quad (4-37)$$

The series solution of Eq. (4-37) decays rapidly as n and λ_n increase due to the exponential decay function. Therefore, for times greater than approximately two seconds, the term

$\sum_{n=1}^{\infty} a_n e^{-\alpha \lambda_n^2 t} \sin \lambda_n x$ has negligible effect on the final solution and was neglected. A similar test was

also employed by Sullivan and McDonald [20]. The reduced solution then becomes

$$T(x, t) = \frac{1}{W} [T_2(W, t) - T_1(0, t)]x + T_1. \quad (4-38)$$

Finally, the heat flux is given by

$$q''(t) = -k \frac{dT(x, t)}{dx}. \quad (4-39)$$

Substituting Eq. (4-38) into Eq. (4-39) gives

$$q''(t) = -k \left[\frac{1}{W} [T_2(W, t) - T_1(0, t)] \right]. \quad (4-40)$$

A similar solution for the heat flux was also determined by Sullivan and McDonald [20]; however a boundary condition of the second kind was used. The heat flux is a function of time and is spatially independent. The dependence on time originates from the dependence of the measured temperatures on time. It should also be highlighted that based on the uncertainty error analysis that was conducted in Section 3.4, Eq. (4-40) requires the determination of only the dimensional length, W , which will result in a reduction in the propagation of uncertainty error. In the model presented by Sullivan and McDonald [20], two-dimensional lengths (L , d) were required, which results in an increased uncertainty in the measured heat flux.

4.2 ESTIMATION OF LOSSES

4.2.1 Radiation Losses

The model does not take into account radiation heat transfer. Therefore, Eq. (4-40) needs to be corrected for the radiation reflected from the surface and the radiation emitted as it increases in temperature. Sullivan and McDonald [20] performed an energy balance (as shown in Fig. 4-4) on the thermal cube sensor, which yielded the net heat flux measured by the sensor as the incident heat flux minus the reflected and emitted heat flux to give [20]

$$q''_{\text{net}}(t) = q''_{\text{incident}}(t) - q''_{\text{reflected}}(t) - q''_{\text{emitted}}(t). \quad (4-41)$$

The reflected heat flux will depend on the absorptivity of the surface, and it will be assumed to be equal to the emissivity [20]. Furthermore, since the body is opaque, radiation will not transmit through the body. Therefore, the reflected heat flux is

$$q''_{\text{reflected}}(t) = (1 - \varepsilon)q''_{\text{incident}}(t). \quad (4-42)$$

The incident heat flux was found by substituting Eq. (4-42) into Eq. (4-41) to give

$$q''_{\text{incident}}(t) = \frac{1}{\varepsilon} [q''_{\text{net}}(t) + q''_{\text{emitted}}(t)]. \quad (4-43)$$

The temperature of the canister walls will increase over the duration of the test due to the absence of a cooling medium such as water. This will result in radiation heat loss from the canister to the ambient surroundings. To compensate for the radiation heat loss, the Stefan-Boltzmann law [61] was included in the model,

$$q''_{\text{emitted}}(t) = \sigma \varepsilon (T(x, t)^4 - T_{\infty}^4). \quad (4-44)$$

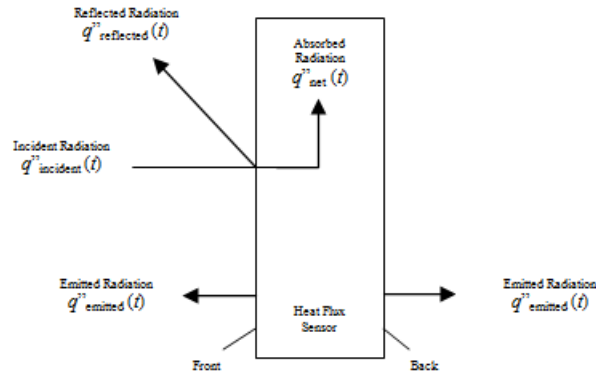


Figure 4-4: The absorption and reflection of incident radiation and emitted radiation of the thermal cube sensor [20]

The incident heat flux on the surface of each of the canister walls then becomes

$$q''_{incident}(t) = -\frac{1}{\varepsilon} \left(\frac{k}{W} [T_2(W, t) - T_1(0, t)] + \sigma \varepsilon [T_2(W, t)^4 + T_1(0, t)^4 - 2T_\infty^4] \right). \quad (4-45)$$

4.2.2 Combustion Exit Losses

The exit losses from the combustion process were quantified based on the energy balance for steady flow systems through the exhaust pipe of the thermal canister similar to the thermal method for calorimeter models (See Section 1.5). The flow of exhaust gases in and out of a control volume through the exhaust pipe is as shown in Fig. 4-5.

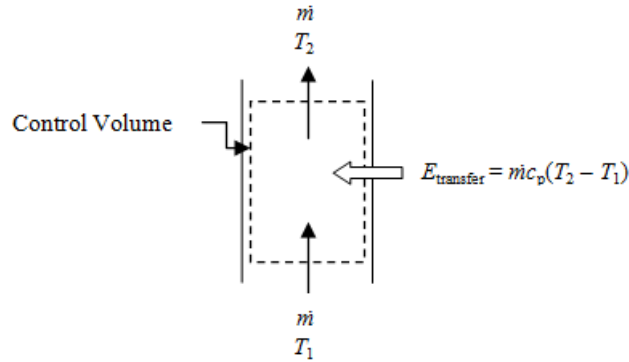


Figure 4-5: Control volume of the energy through the exhaust pipe.

The flow of exhaust gases through the exhaust pipe was assumed to be one-dimensional. As a result, the properties were assumed to be uniform at any cross section normal to the flow direction, and the properties were assumed to have bulk average values over the entire cross section. Under the one-dimensional flow approximation, the mass flow rate through the pipe is expressed as

$$\dot{m} = \rho V A_c, \quad (4-46)$$

where \dot{m} is the mass flow rate of the exhaust gases, A_c is the cross-sectional area of the pipe, ρ is the gas density, and V is the velocity of the exhaust gas. When the changes in kinetic and potential energies are negligible, there is no work, and the energy balance for the steady-flow system reduces to,

$$q'(t) = \dot{m} c_p T = \rho c_p V A_c \Delta T_e, \quad (4-47)$$

where $q'(t)$ is the rate of net heat transfer out of the control volume corresponding to the energy losses from the combustion process, c_p is the specific heat capacity of air, and ΔT_e is the temperature difference between the control volume. To determine the losses experimentally, a

Pitot tube (Dwyer Instruments International, Michigan City, IN, USA) was utilized. Pitot tubes are also used in other exhaust gas applications [67]. The Pitot formula of Eq. (4-48) can be substituted into Eqn. (4-47), as shown in the equations below:

$$V = \sqrt{\frac{2(P_t - P_s)}{\rho}}, \quad (4-48)$$

where, P_t is the total pressure and P_s is the stagnation pressure. $(P_t - P_s)$ is determined using the Pitot tube. Therefore,

$$q'(t) = \rho c_p A_c \sqrt{\frac{2(P_t - P_s)}{\rho}} \Delta T_c. \quad (4-49)$$

4.2.3 Total Heat Release Rate

In order to determine the total heat release from the combustion process, it is required that the incident heat flux to each section of the canister wall be converted to heat flow, q' . The heat flow is defined as

$$q'(t) = q''(t)A_s, \quad (4-50)$$

where A_s is the surface area of the canister wall. Therefore, substituting Eq. (4-45) in Eq. (4-50),

$$q'(t) = -\frac{A_s}{\varepsilon} \left(\frac{k}{W} [T_2(W, t) - T_1(0, t)] + \sigma \varepsilon [T_2(W, t)^4 + T_1(0, t)^4 - 2T_\infty^4] \right). \quad (4-51)$$

The thermal canister was divided into 10 sections along the line of symmetry (including the top cover plate). Therefore, the total heat flow to the thermal canister is given by

$$\sum_{i=1}^{10} q'(t) = -\sum_{i=1}^{10} \frac{A_s}{\varepsilon} \left\{ \left(\frac{k}{W} [T_2(W, t) - T_1(0, t)] + \sigma \varepsilon [T_2(W, t)^4 + T_1(0, t)^4 - 2T_\infty^4] \right) \right\}_i. \quad (4-52)$$

The total heat release rate from the entire system is found by adding the convective loss term, and is given as

$$q'_{Total}(t) = \rho c_p A_c \sqrt{\frac{2(P_t - P_s)}{\rho}} \Delta T_c - \sum_{i=1}^{10} \frac{A_s}{\varepsilon} \left\{ \left(\frac{k}{W} [T_2(W, t) - T_1(0, t)] + \sigma \varepsilon [T_2(W, t)^4 + T_1(0, t)^4 - 2T_\infty^4] \right) \right\}_i. \quad (4-53)$$

As described in detail in Chapter 3, to reduce the propagation of errors, the thermocouples can be modified to use experimentally measured differential wall temperatures, ΔT_w

$$\Delta T_w = T(W, t) - T_1(0, t). \quad (4-54)$$

Therefore the total heat release rate in the thermal canister is given as

$$q'_{Total}(t) = \rho c_p A_c \sqrt{\frac{2(P_t - P_s)}{\rho}} \Delta T_c - \sum_{i=1}^{10} \frac{A_s}{\varepsilon} \left\{ \left(\frac{k}{W} \Delta T_w + \sigma \varepsilon [T_2(W, t)^4 + T_1(0, t)^4 - 2T_\infty^4] \right) \right\}_i. \quad (4-55)$$

4.3 THERMAL CANISTER MODEL VALIDATION

An analysis of the temperature distribution in a section of the thermal canister wall was conducted to determine the accuracy of the incident heat flux values estimated from the mathematical model in Eq. (4-45). The mathematical model was used to estimate the incident heat flux from a transient temperature distribution and compared with the heat flux estimated from the mathematical model by Sullivan and McDonald [20]. The experimental data used in this validation was acquired from an actual simulated test where a transient heat load was applied to the custom-built heat flux sensors. Figure 4-6 shows the result of the incident heat flux

estimated by the thermal canister model compared with the heat flux estimated by the Sullivan and McDonald [20] model. Both models estimated a transient heat flux over the specified time period. The maximum heat flux predicted by the Sullivan and McDonald sensor was 15 kW/m^2 and the thermal canister model predicted a maximum 12 kW/m^2 . The results indicated that the canister model was in close agreement with the thermal cube model. It was observed however, over the time period, the thermal canister model showed signs of lagging when estimating the incident heat flux. This can be attributed to the lower thermal conductivity of Aluminum 6061 (167 W/mK) for the thermal canister compared to the thermal conductivity of Aluminum 6063 T-6 (240 W/mK) for the Sullivan and McDonald sensor, which resulted in a slower response time for the thermal canister.

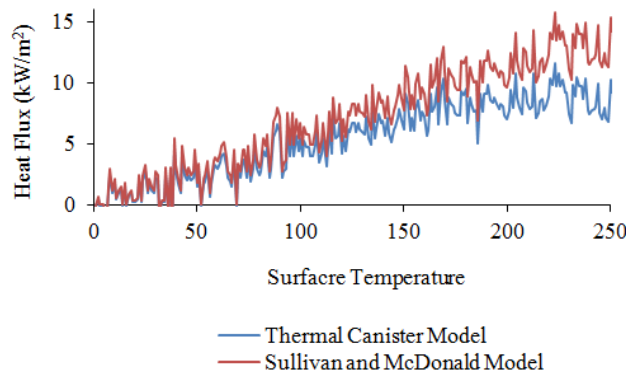


Figure 4-6: Predicted results from the thermal canister model vs. the thermal cube model

The analysis performed validates the accuracy of the heat flux estimation from the thermal canister mathematical model when compared to FEM simulations and the thermal cube model by Sullivan and McDonald. It is therefore recommended that experimental validations be performed for determining the accuracy of the total heat release model in Eq. (4-55).

5. CONCLUSIONS

To improve on the design of the heat flux sensor developed by Sullivan and McDonald [20], which produced large errors in the estimates of incident heat flux, the method of differential temperature measurements was implemented. The incident heat flux data obtained from the modified sensor was found to be on the same order of magnitude as that of the original sensor developed by Sullivan and McDonald [20] and that of a commercial Schmidt–Boelter gauge. There was a noted reduction in noise in the heat flux data and also variations in the transient incident heat flux from the modified sensor were noticeably lower than those of the sensor developed by Sullivan and McDonald [20].

To expand on the capabilities of this modified sensor, a test methodology for comparing the effectiveness of various wildland fire chemical treatments was developed to determine the time-to-ignition of foliar vegetative fuel samples. From the experiments conducted, it was possible to determine the time to flaming ignition from the incident heat flux data, which was validated with transient mass loss data. However, both the heat flux and transient mass loss data were not suitable to determine the time to glowing ignition given the high level of noise in the data before occurrence of flaming combustion. A comparison of the results obtained from the transient heat flux and mass loss data showed that the time to flaming ignition was in agreement to within less than 2% for both measurement systems, which validates the ignition time obtained. There was a slight delay in the ignition time for transition from glowing ignition to flaming ignition due to the physical and chemical burning process of the vegetative fuels. Statistical analysis using a two-sided t-test indicated that the results from the burn test were statistically different for the various chemical treatments. This indicated that the test methodology allowed for effective

differentiation between the wildland fire chemical treatments by comparing their mean ignition times. The narrow standard deviations of the average ignition times suggested that the test methodology was able to produce repeatable results.

The test methodology highlighted in this study may be considered as a feasible alternative for situations in which visual measurements may prove to be onerous and prohibitive. In addition to providing ignition data, this test would contemporaneously provide incident heat flux and transient mass loss data, which may reduce the time required to perform these individual tests. Furthermore, from an applications perspective, the improved heat flux sensor may be used in building alarm and warning systems to supply heat flux data to those systems. This type of system application of the sensor would be particularly useful in buildings that are located within close proximity to wildland forests at wildland–urban interfaces.

Based on the concept of the thermocouple-based heat flux sensor, a thermal calorimeter, “The Thermal Canister,” was developed. For product evaluation purposes, the incident heat flux from the wildfire chemicals evaluation would not be considered an important property as it may vary based on the orientation of the heat flux sensor in relation to the burning sample. Therefore measuring the heat release rate during the combustion process would be a more viable option. The thermal calorimeter was therefore designed to measure the heat release rate along with the ignition time from the burning fuel. The mathematical model developed for the heat flux portion of the thermal calorimeter was compared with that of the model for the Sullivan and McDonald heat flux sensor [20]. The results indicated that the canister model was in close agreement with the Sullivan and McDonald model. Experimental validation is now required to assess the operability of the thermal canister for measuring the total heat release rate.

6. RECOMMENDATIONS FOR FUTURE WORK

The modified heat flux sensor was shown to be capable of estimating the total heat flux in close agreement with a commercial Schmidt-Boelter gauge. However, the transient response time of the custom heat flux sensor, related to the response of the thermocouples, was not studied in great detail. The transient response is a crucial parameter for rapid response processes encountered in flash fire scenarios. This would require determining a heat transfer solution for the characterization of the thermocouple's transient response by modeling the thermocouple as embedded into a solid block.

The modified thermocouple arrangement also resulted in significant reduction in errors of the heat flux estimates. However, these errors were determined using the most conservative scenario based on the manufacturer's stated limit of error for the thermocouples that were used in the study. Therefore, the errors in the heat flux estimates may actually be significantly lower. To determine the actual errors in heat flux estimates, determining the actual thermocouple errors would therefore be required. This would involve developing a rigorous calibration procedure, according to industrial standard, to determine the actual errors in the temperature values from the thermocouples used in the heat flux sensor. Also, to allow for final commercial use, the sensor would need to be calibrated according to industrial standards. This may require the design of a calibration system to be implemented in the laboratory and can be done along with the calibration of the thermocouples.

In the evaluation of wildfire chemicals, additional useful data may be possible. The methodology can be modified to measure the rate of spread. The effect on the rate of spread based on the type

of wildland fire chemical applied can be studied. Also, one of the main causes of the variabilities in ignition times of the different chemicals was the application of the chemicals to the sample. A more efficient method of chemical application can be further investigated. Once a suitable application method is developed, the coverage area factor can now be controlled and the influence on the ignition times can now be investigated which may be an important economic factor. Other factors such as moisture content, the vegetative sample type, and stand-off distance also had a significant impact on the ignition times. The influence of each of the factors on the ignition can be investigated using correlation studies that can also include the coverage area of the chemicals. The evaluation tests were an attempt to replicate the conditions in a real fire scenario and as such a constant heat flux from the radiant heater was not performed. The use of constant heat fluxes may now be investigated, to observe the effects on the ignition time.

Experimental validation of the developed thermal canister model is required to be performed. Comparing the performance of the thermal canister with other calorimeters using similar materials is required to test the accuracy of the heat release measurements. Once the model has been validated, a test methodology for evaluating the performance of the wildfire chemicals is to be developed. Investigation into evaluating the performance other materials can also be performed.

7. REFERENCES

- [1] A. Shlisky, J, et al. “Fire, Ecosystems and People: Threats and Strategies for Global Biodiversity Conservation.” GFI Technical Report 2007-2, The Nature Conservancy. Arlington, VA.
- [2] A. L. Westerling, B.P. Bryant, “Climate change and wildfire in California,” *Climatic Change*, Vol. 87 (1), pp. 231–249, 2008.
- [3] X. Wang, D. K. Thompson, G. A. Marshall, C. Tymstra, R. Carr, M. D. Flannigan, “Increasing frequency of extreme fire weather in Canada with climate change,” *Climatic Change*, Vol. 130(4), 2015.
- [4] J. T. Houghton, Y. Ding, D. J. Griggs, M. Noguera, P. J. van der Linden, X. Dai, K. Maskell, C.A. Johnson, “IPCC climate change: the scientific basis,” Cambridge University Press, Cambridge, United Kingdom, 2001.
- [5] S. W. Running, “Is global warming causing more, larger wildfires?” *Science* Vol. 313, pp. 927–928, 2006.
- [6] M. D. Flannigan, B. J. Stock, M. R. Turetsky, B. M. Wotton, “Impact of climate change on fire activity and fire management in the circumboreal forest,” *Global Change Biology* Vol. 15, pp. 549-560, 2009.
- [7] B. J. Stock, B. M. Wotton, M. D. Flannigan, M. A. Fosbert, D. R. Cahoon, J. G. Goldammer, “Boreal forest fire regimes and climate change,” Pages 233-246 in M.

- Beniston and M. M. Verstraete (editors), Remote sensing and climate modeling: synergies and limitations, Kluwer Academic, Dordrecht, Netherlands, 2001.
- [8] M. A. Moritz, M. Parisien, E. Batllori, M. A. Krawchuk, J. Van Dorn, D. J. Ganz, K. Hayhoe, “Climate change and disruptions to global fire activity,” *Ecosphere* Vol. 3 (6), <http://dx.doi.org/10.1890/ES11-00345.1>, 2012.
- [9] G. D. Haddow, J. A. Bullock, D. P. Coppola, “Introduction to Emergency Management (4th ed.),” Elsevier, Burlington, MA, USA, 2011.
- [10] Canadian Wildland Fire Strategy Assistant Deputy Ministers Task Group, “Canadian wildland fire strategy [electronic resource]: a vision for an innovative and integrated approach to managing the risks: a report to the Canadian Council of Forest Ministers,” Canadian Council of Forest Ministers, 2005, Catalogue No. Fo134-1/2005E-PDF, pp. 1-5, 2005.
- [11] M. D. Flannigan, M. A. Krawchuk, W. J. de Groot, B. M. Wotton, L. M. Gowman, “Implications of changing climate for global wildland fire,” *Intl. J. of Wildland Fire*, Vol. 18, pp. 483–507, 2009.
- [12] J. H. Scott, E. D. Reinhardt, “Assessing crown fire potential by linking models of surface and crown fire behavior,” Research Paper RMRS-RP-29. Fort Collins, CO, U.S. Department of Agriculture, Forest Service, Rocky Mountain Research Station. 59 p., 2001.
- [13] J. R. Holton, J. A. Curry, J. A. Pyle, “Encyclopedia of Atmospheric Sciences, Volumes 1-6 – Wildfire Weather,” Elsevier ISBN 978-0-12-227090-1, 2003

- [14] D. Frankman, B. W. Webb, B. W. Butler, D. Jimenez, J. M. Forthofer, P. Sopko, K. S. Shannon, K. J. Hiers, R. D. Ottmar, "Measurements of convective and radiative heating in wildland fires," *Int. J. Wildland Fire*, Vol. 22 (2), pp. 157–167, 2013.
- [15] G. M. Byram, "Combustion of forest fuels," In: K. P. Davis (editor) "Forest fire: control and use," McGraw-Hill, New York, NY, pp. 61-89, 1959.
- [16] L. A. Salazar, L. S. Bradshaw, "Display and interpretation of fire behavior probabilities for long-term planning," *Environmental Management*, Vol. 10, pp. 393–402, 1986.
- [17] K. G. Hirsch, D. L. Martell, "A review of initial attack fire crew productivity and effectiveness," *Int. J. Wildland Fire*, Vol. 6 (4), 199–215, 1996.
- [18] R. O. Weber, "Wildland fire spread models. In: 'Forest Fires: Behavior and Ecological Effects,'" E. A. Johnson, K. Miyanishi (editors), Academic Press, San Diego, CA, pp. 151–169, 2001.
- [19] J. E. Keeley, "Fire intensity, fire severity and burn severity: a brief review," *Int. J. Wildland Fire*, Vol. 18, pp. 116-126, 2009.
- [20] E. Sullivan, A. McDonald, "Mathematical Model and Sensor Development for Measuring Energy Transfer from Wildland Fires", *Int. J. Wildland Fire*, Vol. 23, pp. 995–1004, 2014.
- [21] C. J. Wieczorek and N. A. Dembsey, "Human Variability Correction Factors for Use with Simplified Engineering Tools for Predicting Pain and Second Degree Burns," *Journal Of Fire Protection Engineering*, vol. 11, no. 2, p. 88, 2001.

- [22] C. T. Kidd, C. G. Nelson, “How the Schmidt-Boelter gage really works,” *Proc. of 41st Int. Instrum. Symp.*, Research Triangle Park, NC, pp. 347-368, 1995.
- [23] R. Gardon, “An instrument for the direct measurement of intense thermal radiation,” *Rev. Sci. Instrum.*, Vol. 24, pp. 366-370, 1953.
- [24] T. E. Diller, “Advances in Heat Flux Measurements,” In: “Advances in Heat Transfer, Vol. 23,” J.P. Hartnett et al. (editors), Academic Press, Boston, pp. 279–368, 1993.
- [25] A. P. Robbins, P. C. Collier, “Heat Flux Measurements: Experiments and Modelling,” BRANZ Study Report 206, BRANZ Ltd, Judgeford, New Zealand, 2009.
- [26] N. R. Keltner, J. V. Beck, J. T. Nakos, “Using Directional Flame Thermometers for Measuring Thermal Exposure,” *J. of ASTM International*, Vol. 7 (2), pp. 27-43, 2010.
- [27] C. Lam, E. Weckman, “Steady-state heat flux measurements in radiative and mixed radiative-convective environments,” *Fire and Materials*, Vol. 33 (7), pp. 303-321, 2009.
- [28] M. L. Samuel, P. Seul-Hyun, C. G. Thomas, “Development of rapidly deployable instrumentation packages for data acquisition in wildland–urban interface (WUI) fires,” *Fire Safety Journal*, Vol. 45 (5), pp. 327-336, 2010.
- [29] K. D. Kalabokidis, “Effects of wildfire suppression chemicals on people and the environment—a review,” *Global Nest: Int J*, Vol. 2, pp. 129–137, 2000.
- [30] S. Liodakis, I. Antonopoulos, T. Kakardakis, “Evaluating the use of minerals as forest fire retardants,” *Fire Safety J*, Vol. 45, pp. 98–105, 2010.

- [31] S. Liodakis, D. Bakirtzis, A. P. Dimitrakopoulos, “Auto ignition and thermogravimetric analysis of forest species treated with fire retardants,” *Thermochim Acta*, Vol. 399, pp. 31–42, 2003.
- [32] J. W. Lyons, “The chemistry and uses of fire retardants,” Malabar, FL: RE Krieger Publishing Company, 1987.
- [33] A. A. Pappa, N. E. Tzamtzis, M. K. Statheropoulos, et al. “A comparative study of the effects of fire retardants on the pyrolysis of cellulose and *Pinus halepensis* pine-needles,” *J Anal Appl. Pyrol*, Vol. 31, pp. 85–100, 1995.
- [34] A. D. Pouwels, G. B. Eijkel, J. J. Boon, “Curie-point pyrolysis–capillary gas chromatography high resolution mass spectrometry of micro crystalline cellulose,” *J Anal Appl Pyrol*, Vol. 14, pp. 237–280, 1989.
- [35] Q. Wang, J. Li, E. Winandy, “Chemical mechanism of fire retardance of boric acid on wood,” *Wood Sci Technol*, Vol. 38, pp. 375–389, 2004.
- [36] ASTM E1321-13. Standard test method for determining material ignition and flame spread properties. West Conshohocken, PA: ASTM International, 2013.
- [37] United States Department of Agriculture (USDA) Forest Service, Wildland Fire Chemical Systems. Standard test procedure, section 2: fire tests, STP 2.1–2.2, <http://www.fs.fed.us/rm/fire/wfcs/tests/index.htm>
- [38] A. M. Tafreshi, M. Di Marzo, “Foams and gels as fire protection agents,” *Fire Safety J*, Vol. 33, pp. 295–305, 1999.

- [39] M. A. Dietenberger, A. Shalbafan, J. Welling, et al. “Treated and untreated foam core particleboards with intumescent veneer: comparative analysis using a cone calorimeter,” *J. Therm Anal Calorim*, Vol. 114, pp. 979–987, 2013.
- [40] D. K. Shen, M. X. Fang, W. K. Chow, “Ignition of wood based materials by thermal radiation,” *Int. J. Eng Perform Based Fire Code*, Vol. 8(2), pp. 69–83, 2006.
- [41] S. McAllister, L. Grenfell, A. Hadlow, et al. “Piloted ignition of live forest fuel,” *Fire Safety J*, Vol. 51, pp. 133–142, 2012.
- [42] National Fire Protection Association. NFPA 2113: standard on selection, care, use, and maintenance of flame-resistant garments for protection of industrial personnel against flash fire, 2015.
- [43] N. Ayrilmis, Z. Candan, R. White, “Physical, mechanical, and fire properties of oriented strand board with fire retardant treated veneers,” *Holz Als Roh-Und Werkst*, Vol. 65, pp. 449-458, 2007.
- [44] ISO 5660-1:1993. Fire tests—reaction to fire. Part 1—rate of heat release for building products (cone calorimeter method).
- [45] ASTM E1354-02. Standard test method for heat and visible smoke release rates for materials and products using an oxygen consumption calorimeter. West Conshohocken, PA: ASTM, 2002.
- [46] O. Grexa, H. Lubke, “Flammability parameters of wood tested on a cone calorimeter” *Polym Degrad Stabil*, Vol. 74, pp. 427–432, 2001.

- [47] Specification for Long Term Retardant, Wildland Firefighting, United States Department of Agriculture Forest Service: Specification 5100-340c, 2010.
- [48] Specification for Fire Suppressant Foam (Class A. Foam) for Wildland Firefighting, United States Department of Agriculture Forest Service: Specification 5100-307a, 2010.
- [49] Specification for Water Enhancers (Gels) for Wildland Firefighting, United States Department of Agriculture Forest Service: Specification 5100-306a, 2010.
- [50] M. L. Janssens, "Methods and Equations of Fire Calorimetry," In M. M. Hirschler, R. E. Lyon (eds.), Special Symposium on Fire Calorimetry, Gaithersburg, MD, July 27-28, 1995, pp.11-22.
- [51] W. M. Thornton, "The Relation of Oxygen to the Heat of Combustion of Organic Compounds," *Philos. Mag.*, Ser. 6 (33), 196-203 (1917).
- [52] E. Sullivan, "Measuring Energy Transfer from Wildland Forest Fires," University of Alberta, MSc. Thesis, 2014.
- [53] J. R. Taylor, "An Introduction to Error Analysis: The Study of Uncertainties in Physical Measurements," 2nd ed., Sausalito, California: University Science Books, pp. 13, 60-66, 1996.
- [54] R. Powell, W. Hall, C. Hyink, L. Sparks, G. Burns, M. Scroger, H. Plumb, "Thermocouple Reference Tables Based on the IPTS-68," Stamford, Connecticut: Omega Press, pp. 350.
- [55] X. Silvani, F. Morandini, "Fire spread experiments in the field: Temperature and heat fluxes measurements," *Fire Safety J*, Vol. 44 (2), pp. 279 – 285, 2009.

- [56] ASTM D4442-07, Standard Test Methods for Direct Moisture Content Measurement of Wood and Wood-Base Materials, ASTM International, West Conshohocken, PA, 2007.
- [57] Omegalux QF, QG, QC, and QH Series Infrared Radiant Panel, Operator's Manual, Omega Engineering Incorporated, 1991.
- [58] T. L. Bergman, A. S. Lavine, F. P. Incropera, D. P. DeWitt, "Fundamentals of Heat and Mass Transfer," 7th Edition, John Wiley & Sons, Inc., Hoboken, NJ, pp. 862 – 870, 2011.
- [59] R. W. Powel, C. Y. Ho, P. E. Liley, "Thermal Conductivity of Selected Materials", National Standard Reference Data Series – National Bureau of Standards – 8 (Category 5 – Thermodynamic and Transport Properties), Issued November 25, 1966.
- [60] L. Jiji, "Heat Convection," 2nd ed., Berlin: Springer, pp. 6, 260-279, 2209.
- [61] Y. A. Çengel, A. J. Ghajar, "Heat and Mass Transfer: Fundamentals & Applications," 4th ed., New York: McGraw-Hill, 2011, pp. 12 – 14, 237, 249, 527, 753, 884.
- [62] A. McDonald, C. Moreau, S. Chandra, "Use of thermal emission signals to characterize the impact of fully and partially molten plasma-sprayed zirconia particles on glass surfaces," *Surface and Coating Technology*, Vol. 204, 2323 – 2330, 2010.
- [63] D. C. Montgomery, "Design and Analysis of Experiments," 8th Edition, John Wiley and Sons, Inc., Arizona, pp. 36-38, 686, 2013.
- [64] L. Jiji, "Heat Conduction," 3rd ed., Springer-Verlag Berlin Heidelberg, Inc., pp. 72–83, 120–128, 2009.

- [65] J. Bray, "Aluminum Mill and Engineered Wrought Products, Properties and Selection: Nonferrous Alloys and Special-Purpose Materials," in ASM Handbook, vol. 2, ASM International, pp. 29-61, 1990.
- [66] Y. S. Touloukian, "Thermophysical properties of matter: Thermal Conductivity: Metallic Elements and Alloys," New York: IFI/Plenum, pp. 1, 908-909, 1970.
- [67] H. Nakamura, I. Asano, M. Adachi, J. Senda, "Analysis of pulsating flow measurement of engine exhaust by a Pitot tube flowmeter," *Int. J. Engine Res.* Vol. 6 (1), pp 85–93, 2005.
- [68] D. G. Chavers., F. R. Chang-Diaz, C. Irvine, J. P. Squire, "Momentum and Heat Flux Measurements in the Exhaust of VASIMR using Helium Propellant," NASA Technical Documents, NASA Johnson Space Center, Marshall Space Flight Center, ID 20030063051, 2013.

2. Omega Radiant Heater Specifications [56]

SECTION 5 SPECIFICATIONS

5.1 GENERAL SPECIFICATIONS

VOLTAGE:

QF SERIES: 120 VAC, 480 VAC, 1 and 3 phase
120/240, 240/480 VAC dual voltage, 1 phase

QG SERIES: 120, 240 and 480 VAC, 1 phase
120/240, 240/480 VAC dual voltage, 1 phase

QC, QH SERIES: 240 VAC, 1 phase
240/480 VAC dual voltage, 1 phase

WATTAGE:

QF SERIES: 720 - 21,600 watts

QG SERIES: 720 - 8640 watts

QC, QH SERIES: 1660 - 8640 watts

MAXIMUM OPERATING TEMPERATURE:

QF, QG SERIES: 1600°F

QC, QH SERIES: 1800°F

DIMENSIONS: See specific Series specifications in Sections 5.2 through 5.4.

Omega Radiant Heater Specifications [56]

5.4 QC AND QH SERIES

The warm up curve (Figure 5-5) shows the response time of the QC and QH Series infrared heaters, measured by a thermocouple from a cold start to a maximum temperature. Changes in temperature, or partial warm up will be approximately this curve.

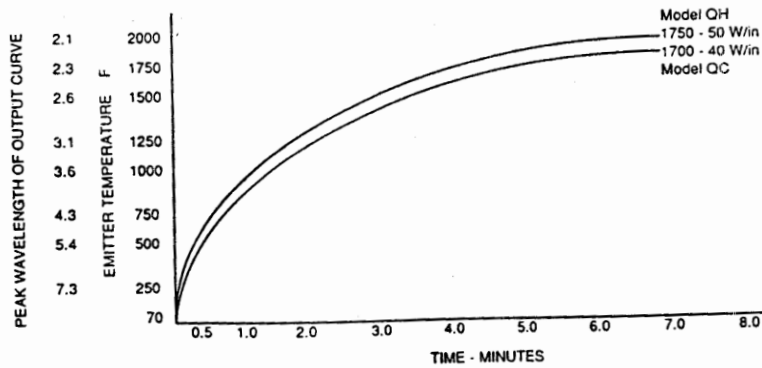


Figure 5-5. Warm Up Curve

The emission output curve (Figure 5-6) compares the emitter face temperature versus the corresponding wavelength emitted for a specific temperature. The key to efficiency is to select an emitter wavelength that best matches the peak absorption of the process product.

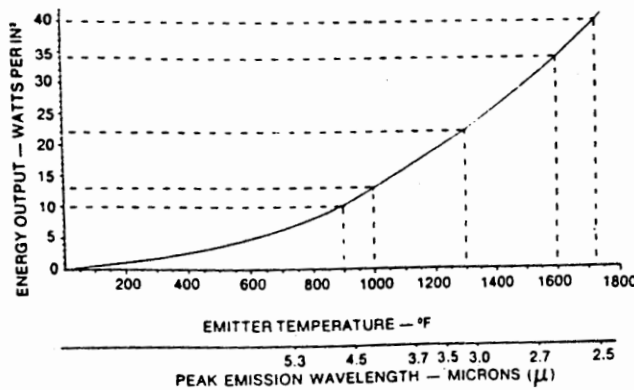
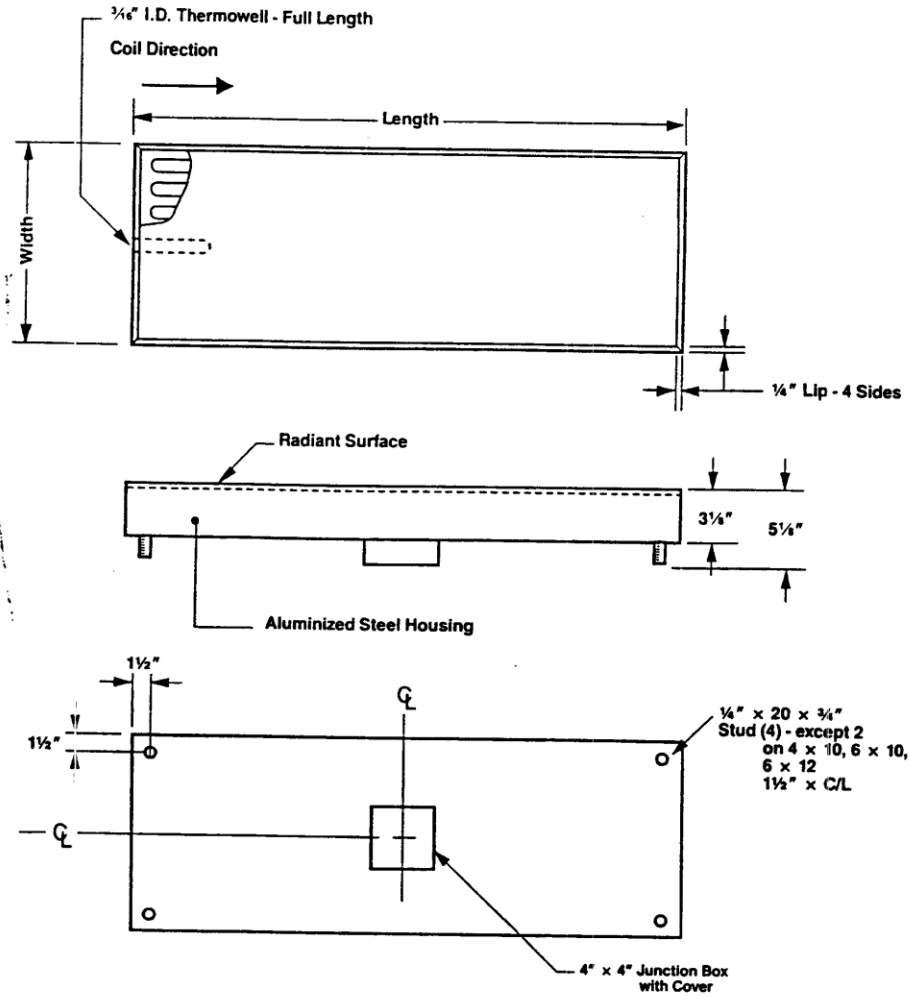


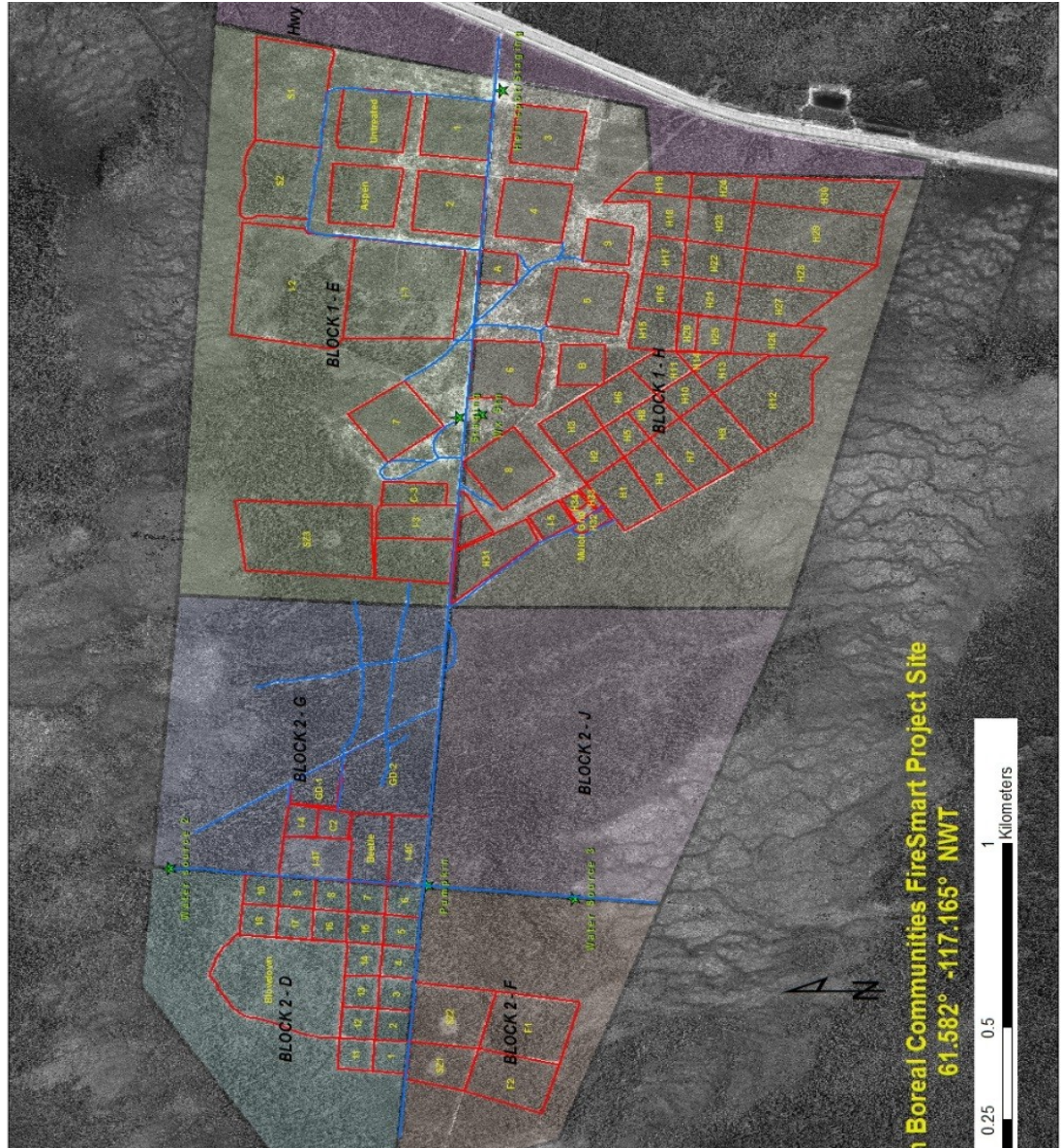
Figure 5-6. Emission Output Curve

Omega Radiant Heater Specifications [56]



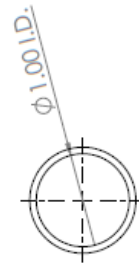
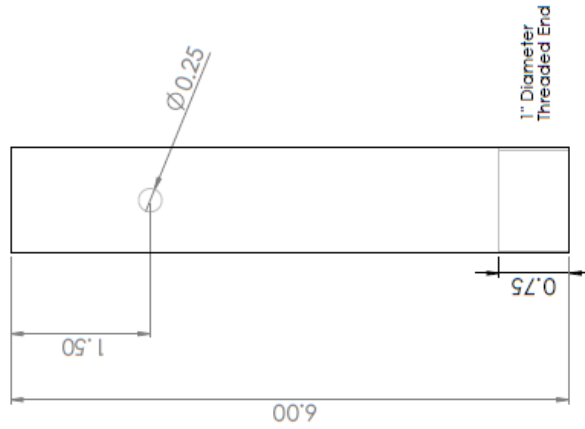
Width (in.)	Length (in.)	Wattage	Voltage	Phase	Without Thermowell	With Thermowell
					Model No.	Model No.
40 W/in² QC Series						
4	10	1600	240	1	QC-041040	QC-041040-T
6	10	2400	240/480	1	QC-061040	QC-061040-T
8	10	3200	240/480	1	QC-081040	QC-081040-T
10	10	4000	240/480	1	QC-101040	QC-101040-T
12	10	4800	240/480	1	QC-121040	QC-121040-T
6	12	2880	240/480	1	QC-061240	QC-061240-T
12	12	5760	240/480	1	QC-121240	QC-121240-T
60 W/in² QH Series						
4	10	2400	240/480	1	QH-041060	QH-041060-T
6	10	3600	240/480	1	QH-061060	QH-061060-T
8	10	4800	240/480	1	QH-081060	QH-081060-T
10	10	6000	240/480	1	QH-101060	QH-101060-T
12	10	7200	240/480	1	QH-121060	QH-121060-T
6	12	4320	240/480	1	QH-061260	QH-061260-T
12	12	8640	240/480	1	QH-121260	QH-121260-T

3. Canadian Boreal Communities FireSmart Project Site



ITEM NO.	DESCRIPTION	MTL	QTY.
1	1" Diameter Tube	Aluminum	1

ALL DIMENSIONS IN INCHES



UNLESS OTHERWISE SPECIFIED, DIMENSIONS ARE IN INCHES		TITLE		DO NOT SCALE DRAWING		REGION	
SCALE	DATE	DESIGNED BY	DATE	CHECKED BY	DATE	DESIGN NO.	SHEET NO.
DATE	DATE	DATE	DATE	DATE	DATE	Aluminum Tube	43
MATERIAL: Aluminum Tube							Thermal Canister
MATERIAL: Aluminum Tube							Exhaust Pipe
MATERIAL: Aluminum Tube							A3
MATERIAL: Aluminum Tube							SHEET 1 OF 1